EDITORIAL BOARD

REGISTER

https://doi.org/10.26552/aer.C.2020.2.1

DESIGN PROCEDURE AND HONEYCOMB SCREEN IMPLEMENTATION TO THE AIR TRANSTPORT DEPARTMENT'S SUBSONIC WIND TUNNEL

Michal Hrúz
Air Transport Department
University of Žilina
Univerzitná 8215/1
010 26, Žilina
michal.hruz@stud.uniza.sk

Pavol Pecho
Air Transport Department
University of Žilina
Univerzitná 8215/1
010 26, Žilina
pavol.pecho@fpedas.uniza.sk

Martin Bugaj
Air Transport Department
University of Žilina
Univerzitná 8215/1
010 26, Žilina
martin.bugaj@fpedas.uniza.sk

Abstract

Wind tunnels are the most widely used tools when comes to validation of Reynold number. Most of wind tunnels use various air straighteners or flow conditioners to achieve as most unified air flow as it's possible. This article deals with design and creation procedure of air flow straightener – honeycomb screen. Based on mathematical relations and empirical experience defines dimensions and characteristics for subsonic wind tunnel of the Air Transport Department of University of Žilina. Wind tunnel equipped with a suitable screen provides more relevant and accurate data, which are crucial for final validation of results of test objects.

Keywords

honeycomb, air straightener, flow conditioner, flow straightener, screen, wind tunnel

1. Introduction

The wind tunnel is a tool to study fluid flows around a body and the forces generated by the fluid-structure interaction (Panda & Samanta, 2016). The main concerns of aircraft aerodynamics are reducing drag, reducing noise, and improving lift forces on aerodynamic objects (Łusiak, 2020). Wind tunnels are used as a key tool in various engineering applications such as building aerodynamics, study of boundary layers, simulation of atmospheric layers, small-scale testing of aircraft/vehicle models and subsequent validation of numerical predictions They offer a rapid, economical, and accurate means for aerodynamic research (Kulkarni et. al., 2011).

The Reynolds (Re) number is a quantity which engineers use to estimate if a fluid flow is laminar or turbulent. This is important, because increased mixing and shearing occur in turbulent flow. The Reynolds number is calculated using mean velocity, pipe diameter, density, and viscosity, and is valid for any fluid. The Reynolds number is also dependent upon the geometry of the pipe, as well as the roughness of the walls. Yet, no successful analytical methods for determining the Reynolds number have been developed due largely to the difficulty associated with predicting turbulent flow, and so Reynolds numbers for flow through pipes or around immersed objects must be determined experimentally (Yang, 2012).

In view of this necessity, a subsonic wind tunnel has been installed at Žilina Airport in Dolný Hričov in the year 2020. The layout of this tunnel with the dimensions of various components is shown in Fig. 1.

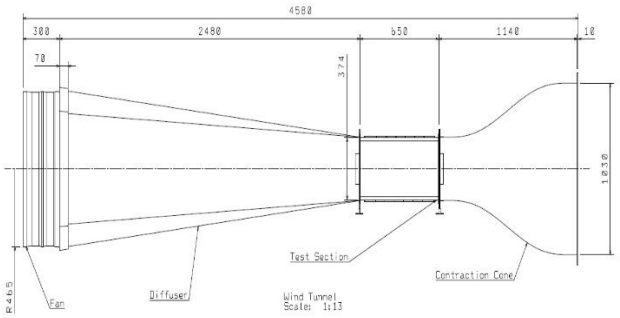

Figure 1: Layout of the subsonic wind tunnel at Žilina Airport, Dolný Hričov. Source: Authors.

It is an open-circuit type wind tunnel with a square test section of 0.35 x 0.35 m² and 0.650 m length. Air flow is established in the test section by using an axial fan powered by 400 W electric motor. This subsonic wind tunnel consists of four segments or sections. The inlet section and diffuser are made of laminated wood. The process of lamination was done with the usage of five levels of plywood, which were glued together in special forms in order to establish curved profiles.

In terms of simplicity of construction and economy, the bearing structure of the test section, which is shown in Fig. 2., is composed of aluminium strips, which were welded to the desired profile. To ensure thorough visibility of the air flow inside, the walls of the test section are fitted with LED light elements and acrylic glass, which reinforces the structure and dampens possible vibration.

Generally, in order to achieve better performance in terms of laminar flow in the test section various methods can be

applied. The air straighteners or screens are often used mainly to minimize the turbulence level in the test section.

According to (Škultéty, 2018), the lower the Reynolds number the more laminar airflow can be expected.

Figure 2: Transparent test section. Source: Authors.

The screens cascade large-scale turbulent fluctuations into smaller scales. These decay in the settling duct must be sufficiently long to allow sufficient decay, while minimizing boundary-layer growth (Cattafesta, 2010).

According to (Kulkarni et. al., 2011) honeycomb is a passage of ducts, laid along the axis of the main air stream to suppress the cross velocity components, which are initiated during the swirling motion in the air flow during entry, The cross-sectional shapes of honeycombs may be square, circular and regular hexagonal cells, as shown in Fig. 3.

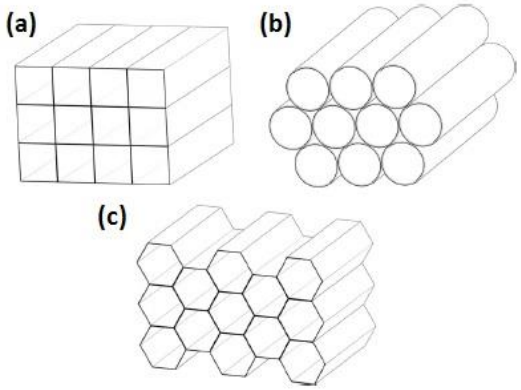

Figure 3: Schematic of several honeycomb cross-sections including square (a), circular (b) and regular hexagonal cell (c). Source: Kulkarni (2011).

2. Honeycomb design criteria

To improve the relevance of output data, it is necessary to design and create an optimal screen suited for the conditions of this wind tunnel.

According to (Metha & Bradshaw, 1979), as far as the design method is concerned, the honeycomb length, the cell hydraulic and the porosity are design key factors.

The honeycomb porosity is the ratio between the actual flow cross-section area and the total cross-section area, and it is expressed by Eq. (1).

$$\beta_h = \frac{\Omega_{Flow}}{\Omega_{tot}} \tag{1}$$

Two main conditions must be verified in the honeycomb design (Metha & Bradshaw, 1979). The honeycomb length and cell hydraulic diameter ratio must be in the range between 6 and 8 and the honeycomb porosity should be greater than 0.8 (see Eq. (2) and Eq. (3))

$$6 \leq \frac{L_{honey}}{d_{honey}} \leq 8 \tag{2}$$

$$\beta_h \geq 0.8 \tag{3}$$

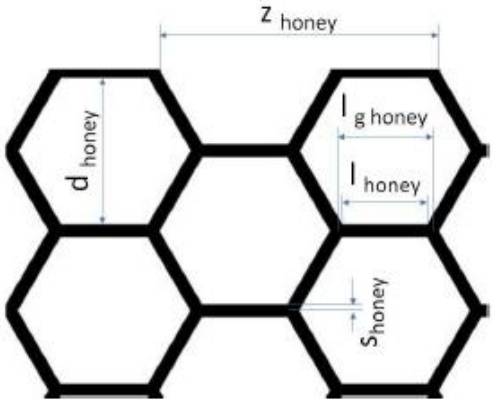

Figure 4: Honeycomb structure dimensions. Source: Mauro (2017).

As shown in Fig. 4, the honeycomb screen is defined by its geometric dimensions such as: inside honeycomb cell length l_{honey}; outside honeycomb cell length $l_{g\ honey}$; honeycomb cell diameter d_{honey}; honeycomb cell thickness S_{honey}; honeycomb solid sheet divisions z (Mauro, 2017).

The internal and external honeycomb cell lengths may be determined thorough Eq. (4) and Eq. (5), respectively.

$$l_{honey} = \frac{d_{honey}}{2 \sin 60°} \tag{4}$$

$$l_{g\ honey} = l_{honey} + 2\frac{S_{honey}}{\tan 60°} \quad (5)$$

The solid sheet divisions can be evaluated using the same method (see Eq. (6)).

$$z_{honey} = 2\ l_{honey} + 2\ l_{g\ honey} \quad (6)$$

In order to calculate the solid area of the honeycomb, considering a single division, the solid area is the sum of two rectangular areas and two trapezoidal areas (see Fig. 3.). These areas can be calculated using Eq. (7) and Eq. (8).

$$S_{trapeze} = l_{honey}\ S_{honey} \quad (7)$$

$$S_{trapeze} = \frac{(l_{honey} + l_{g\ honey})\ S_{honey}}{2}\ l_{honey} + l_{g\ honey} \quad (8)$$

To determine the honeycomb porosity, it is necessary to determine the number of divisions height-wise and width-wise. The number of divisions height-wise is defined as the ratio between the settling chamber cross-section height and the honeycomb divisions, as showed in Eq. (9).

$$n_z = \frac{h_{SC}}{z_{honey}} \quad (9)$$

The number of divisions width-wise is the ratio between the settling chamber cross-section width and the sum of honeycomb cell thickness and the half honeycomb cell diameter (see Eq. (10)).

$$n_{sheet} = \frac{L_{SC}}{h_{SC} + \frac{d_{honey}}{2}} \quad (10)$$

It is evident that for square cross-sections Eq. (11) comes out.

$$h_{SC} = L_{SC} \quad (11)$$

Therefore, the cross-section area of the honeycomb solid sheet is calculated using Eq. (12).

$$\Omega_{sheet} = 2\ (S_{rectangle} + S_{trapeze})\ n_z\ n_{sheet} \quad (12)$$

In a dual way, it is possible to define the honeycomb solidity as the ratio between the cross-section area of the solid sheet and the settling chamber cross-section area. According to the solidity definition, Eq. (13) comes out.

$$\sigma_h = \frac{\Omega_{sheet}}{\Omega_{tot}} \quad (13)$$

Comparing Eq. (13) and Eq. (19), it is easy to achieve the conclusion that the honeycomb and porosity are complementary factors. Thus, Eq. (14) comes out.

$$\sigma_h + \beta_h = 1 \quad (14)$$

Therefore, knowing the honeycomb solidity, the porosity can be calculated using Eq. (14). Thus, the criterion expressed in Eq. (3) is verified.

The design criterion in Eq. (2) should be verified. Thus, the cell hydraulic diameter should be calculated. Firstly, the cell area is calculated using Eq. (15).

$$\Omega_{cell} = 6\left(\frac{d_{honey}}{2}\frac{l_{honey}}{2}\right) = 6\frac{d_{honey}}{2}\frac{d_{honey}}{2\sqrt{3}} = \frac{3}{2}\frac{d_{honey}^2}{\sqrt{3}} \quad (15)$$

Areas equality is used (see Eq. (16)) to determine the cell hydraulic diameter.

$$\pi\frac{D_{h\ honey}^2}{4} = \Omega_{cell} = \frac{3}{2}\frac{d_{honey}^2}{\sqrt{3}} \quad (16)$$

Thus, Eq. (17) comes out and the cell hydraulic diameter can be obtained.

$$D_{h\ honey} = d_{honey}\sqrt{\frac{6}{\pi\sqrt{3}}} \quad (17)$$

It should be noted, that both criteria expressed by Eq. (2) and Eq. (3) must be verified at the end of the honeycomb design procedure.

3. Installation criteria

Final screen was placed into straight section which is part of the inlet section. The straight section provides almost 0.14 m long space right in front of the test section. The diameter of the straight section is the same as the test section, 0.35 x 0.35 m.

Based on the mentioned in the previous chapter, the final dimensions of honeycomb were set as is shown in Tab. 1. and Fig. 5.

Table 1: Final dimensions of honeycomb screen. Source: Authors.

Criteria	**Value**
Criterion 1. Eq. (2)	$6 \leq \underline{7.5} \leq 8$
Criterion 1. Eq. (3)	$\underline{0.94} \geq 0.8$
Screen length	83 mm
l_{honey}	7 mm
lg_{honey}	7.8 mm
d_{honey}	13.6 mm
S_{honey}	0.8 mm

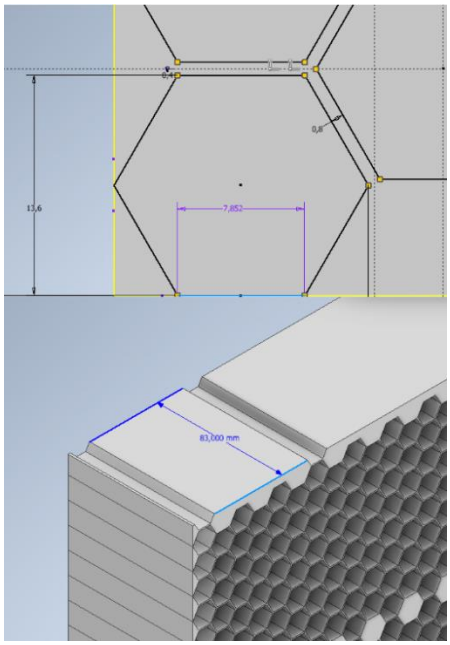

Figure 5: Printing design of honeycomb in PC software Inventor 2019. Source: Authors.

Due to financial costs and simplicity the honeycomb screen itself was 3D printed using FDM method, which is the most frequent method for printing 3D objects such as functional prototypes and concept models (Pecho, 2019). It involves melting the working material and applying it with thin threads one on top of the other. When it freezes, the material binds together to form a hard and durable coating (Iljaszewicz, 2020). Because of the large size of the honeycomb screen, the whole printing process was divided into four individual parts (see fig. 6.).

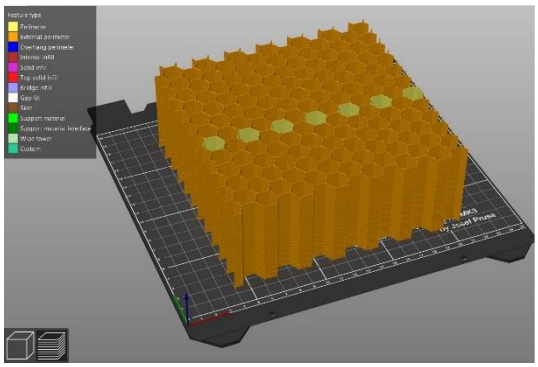

Figure 6: Printing design of one part of four. Source: Authors.

All four parts were glued together and create the final form of honeycomb screen. In order to remove possible roughness after the print, all surfaces were subjected to mechanical treatment.

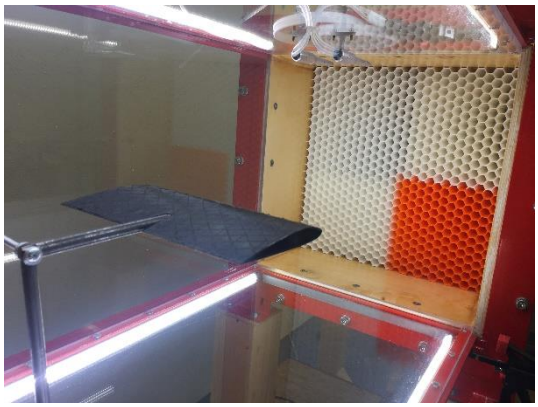

Figure 7: Final form of honeycomb screen installed in straight section. Source: Authors.

Sides of the honeycomb were designed to have tapered profile so it can fit right into a straight section of the inlet section (see Fig. 7.). This option reduced the possibility of vibration or incorrect placement of the screen. In addition, the smoke nozzles are located right behind the air straightener, thus the air mixed with a smoke can easily access to the its cells.

4. Results

Verification of velocity and laminar flow was performed after the installation of honeycomb screen. Verifications were carried out by usage of anemometer, which is a device used for measuring wind speed (air velocity) and in form of visual check.

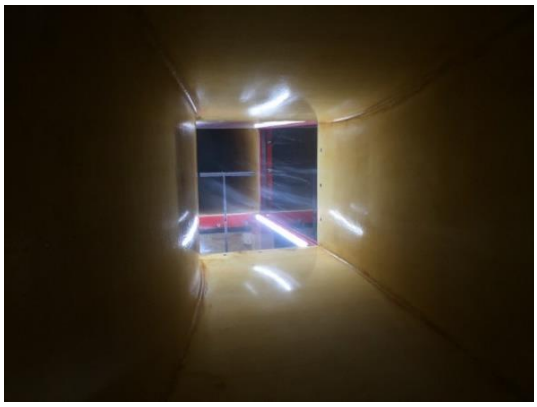

Figure 8: Air flow before the installation of air straightener. Source: Authors.

The Fig. 8. shows how the air flow looked before the installation of air straightener. The air flow is separated. Individual streamlines are separated from each other in the test section all around the tested wing profile, which presents unwanted conditions for relevant outputs of experimental measurement and visual analyses.

Figure 9: Air flow visualisation after the installation of honeycomb screen. Source: Authors.

Installation of honeycomb screen made a significant improvement in the terms of laminar flow inside the test section as we can see in Fig. 9., individual streamlines create one uniform stream or air flow which over floats tested wing profile.

However, the drawback of this improvement is the air velocity loss. The anemometer showed huge reduction of air velocity inside the test section. Before the installation, the wind tunnel could reach speed of almost 11.1 m/s (40 km/h). After the installation, the speed was reduced almost twice. Anemometer showed only 6.9 m/s (25 km/h).

5. Conclusion

In conclusion, it is possible to claim that the main goal was successfully fulfilled. On the other hand, the size of the honeycomb screen itself is responsible for huge air velocity drop inside the test section, mainly because it creates unwanted drag.

In order to achieve higher air velocity inside the test section, it is suggested to replace an axial fan which was powered by 400 W electric motor for a stronger one. The wind tunnel meets the specified criteria for running the experiments. The aim of the paper was to describe the design and structure of the honeycomb screen construction for specific requirements and conditions, specifically for the subsonic wind tunnel of Air Transport Department of The University of Žilina. During the design phase, the authors followed mathematical methods for calculating the dimensions of open-type subsonic wind tunnels.

Future work

A new stronger electric motor is currently being installed along with the frequency converter. The old 400 W electric engine will be replaced for a new 4 kW electric engine. The 10 times stronger fan can provide enough power a thus air velocity for experimental analysis in subsonic wind tunnel.

Acknowledgment

This work was supported under the project of Operational Programme Integrated Infrastructure: *Research and development of contactless methods for obtaining geospatial data for forest monitoring to improve forest management and enhance forest protection*, **ITMS code 313011V465**. The project is co-funding by European Regional Development Fund.

References

Cattafesta, L. & Bahr, C., et. al., Fundamental of Wind-Tunnel design. Encyclopedia of Aerospace Engineering. DOI: 10.1002/9780470686652.eae532

Iljaszewicz, P., Łusiak, T., et. al., 2020. Aerodynamic analysis of the aircraft model made with the 3D printing method. In Transportation Research procedia. ISSN: 2352-1465. Vol. 51. pp. 118-133. Online: https://doi.org/10.1016/j.trpro.2020.11.014.

Kulkarni, V., Sahoo, N., Chavan, S. D., 2011. Simulation of honeycomb-screen combinations for turbulence management in a subsonic wind tunnel. Journal of Wind Engineering and Industrial Aerodynamics. Vol 99. Issue 1. pp. 37-45. ISSN: 0167-6105. Online: https://doi.org/10.1016/j.jweia.2010.10.006.

Łusiak, T., Novak, A., et. al., 2020. Assessment of impact of aerodynamic loads on the stability and control of the gyrocopter model. In Comunications – Scientific Letters of the University of Zilina, Vol. 22 No. 4. pp. 63-69. Online: https://doi.org/10.26552/com.C.2020.4.63-69

Mauro, S., Brusca, S., Lanzafame, R., et. al., 2017. Small-Scale Open-Circuit Wind Tunnel: Design Critecia, Construction and Calibration. International Journal of Applied Engineering Research. Vol 12. Number 23. pp. 13649-13662. ISSN: 0973-4561

Metha, R. D., Bradshaw P., 1979. Design Rules for Small low Speed Wind Tunnels. Journal of Royal Aeronautical Society. Vol. 73. DOI: 10.1017/S0001924000031985

Panda, M. K. & Samanta, A. K., 2016. Design of Low Cost Open Circuit Wind Tunnel – A Case Study. Indian Journal of Science and Technology. Vol 9. ISSN: 0974-6846.

Pecho, P., Ažaltovič, V., et. al., 2019. Introduction of design and layout of UAVs 3D printed wings in relation to optimal

lightweight and load distribution. In Transport Research Procedia. ISSN: 2352-1465. Vol. 40. pp. 861-868. Online: https://doi.org/10.1016/j.trpro.2019.07.121.

Škultéty, F., Badánik, B., et. al., 2018. Design of Controllable Unmanned Rescue Parachute Wing. In Transportation Research Procedia. Vol. 35. pp. 220-229. ISSN: 2352-1465. online: https://doi.org/10.1016/j.trpro.2018.12.026.

Yang, N. K. C., 2012. Design of Wind Tunnel (FLUID FLOW ANALYSIS). Faculty of Manufacturing Engineering. University Malaysia Pahang. pp. 1-24. Online: https://core.ac.uk/download/pdf/159179393.pdf

https://doi.org/10.26552/aer.C.2020.2.2

STUDY OF REINFORCEMENT DESIGN H-PROFILE OF AIRCRAFT WING SPAR

Pavol Pecho
Air Transport Department
University of Zilina
Univerzitná 8215/1
010 26, Žilina
Pavol.pecho@fpedas.uniza.sl

Paulína Magdolenová
Department of Fire Engineering
University of Zilina
Univerzitná 8215/1
010 26, Žilina
Paulina.magdolenova@kpi.fbi.sk

Michal Hrúz
Air Transport Department
University of Zilina
Univerzitná 8215/1
010 26, Žilina
michal.hruz@stud.uniza.sk

Pavel Kováčik
Kobaltsky Welding
Jerichov 26
957 01, Brezolupy
Kobaltsky1@gmail.com

Iveta Škvareková
Air Transport Department
University of Zilina
Univerzitná 8215/1
010 26, Žilina
Iveta.skvarekova@fpedas.uniza.sk

Abstract

In today's world, with ever-increasing safety requirements, there is a growing demand to maintain or reduce production costs. In aviation, in addition to factors like weight and related variables such as resistance to vibration, corrosion, temperature and other are also considered. The task of this paper is to analyse unconventional designs of wing beams with respect to the current requirements of the aviation industry. In the article, the authors analyse the possibilities of design modification either by adding ribs to the profile, or by changing the cross-section of the profile itself. In practice, such design changes would increase weight, production time and finances, but also increase strength and thus safety. All proposed changes were subjected to strength analyses by FEM (Finite element method) computer simulations. The article output is the selection of suitable designs for further observation and experimental verification to ensure comprehensive results for the possibility of implementation in practice. Despite the non-traditional shapes of the proposed wing beam cross-sections, the authors assume that traditional beam shapes will be gradually modified more efficiently.

Keywords

wing spar, wing beam, H-profile, wing design

1. Introduction

Historically, the first flight dates back more than 100 years. Even then, aircraft designers were looking for ways to build solid wings. However, in terms of beam strength, the problem is much older. Beams are the basic element of the longitudinal system of the wing. In the case of purely girder wings, they ensure the full extent of the transmission of bending loads; in the case of girder half-shells, they play a significant role in the bending transmission (Kindmann, 1993). Their weight is in the range of 25 - 50% of the whole wing weight, while higher values relate to beam wings, lower values to half-shells wings (Chen, C.-C, 2019). According to the structural arrangement, we divide the beams into full-walled and, rarely occurring, lattice beams. Like in aviation, as well as in the civil engineering industry beam with I- or H-profile occur. The area of building constructions inspired authors with the ability to drop the collapse risk by adding supporting elements to the beams, for example in the form of ribbing (Figure 1-right) (Abdel-Ghaffar, 2003). The ribbing allows a more efficient distribution of internal material stresses and prevents the beam from collapsing (Figure 1-left).

Figure 10: Detail of the numerical simulation of the steel column collapse with additional ribbing (left) and additional ribs on steel H-profile building structure beam (right). Source: Authors.

In both fields, civil and aerospace engineering, the main effort is focused on prevention of bursts, collapse, or any other damage. To ensure the best mechanical properties, it is necessary to know the position of a beam neutral axis. The neutral axis is a line (more precisely in the spatial concept of the area), which changes the sense of its internal axial effective countervailing forces under bending stress (Figure 3). That means that the best use of the mechanical properties of the beam flange material is in the places furthest from its neutral axis (Nardin, 2009).

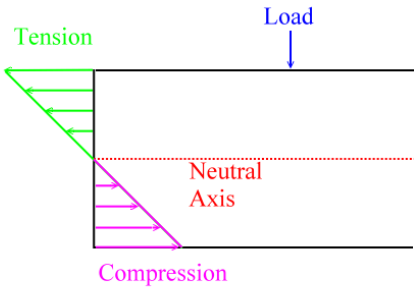

Figure 11: Visualization of the neutral axis at the side looking at the H-profile beam source: Authors.

Assuming the use of the same material and of the same cross-section for both the upper and the lower flange, the neutral axis will lie in the middle of the beam height. For most of the wing beams is, indeed, the material of the two flanges is the same, but usually with different cross-sections. The neutral axis then passes through the common gravity centre of these two flanges and it tends to be closer to the thicker, predominantly of the upper flange (Starší, 2020).

The figure 3 shows a metal embedded beam of a Bf-109 fighter aircraft. The beam has, for the most part of the span, a profile I, near the end of the wing it passes into a profile C. The flanges (1) are made of duralumin L-profiles (3), the cross-section of which decreases towards the wing end. The web (2) is made of duralumin sheet, in the root part thicker, at the end of the wing the sheet is thinner. The rear flange (pictured from the visible side of the beam) degrades from its L-profile to its end in the area between sections A and C only into a vertical shear plate riveted to the web. The front L-profile is terminated even earlier than the rear and passes into the sheet metal flange of the wing end, which is formed by bending the end part of the web into a C-shape. The hinge fittings (5) are made of high-strength steel. The lower hinge is equipped with a ball joint both to reduce the parasitic load on the hinges by operational deformations of the spar, and to facilitate its assembly and disassembly. A number of spacers (6) are arranged along the length of the beam to reinforce the web. These are also used to connect the ribs to the beam. It is worth mentioning the reinforcement (9) of the web in the place of the large hole, which was forced by the cannon installation in the wing. The view of the entire skeleton of the wing is also shown in the Figure 3. The front L-profile is terminated even earlier than the rear and passes into the sheet metal flange at the wing end, which is formed by bending the end portion of the web into the C-shape (Starší, 2020).

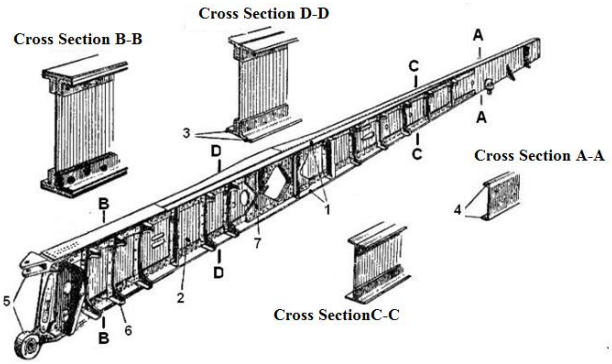

Figure 12: Wing spar of BF-109 airplane. Source: Starší (2020).

Along with the size and shape of the flange cross-section, the mechanical properties of the used material, namely its tensile modulus E, contribute to the final beam stiffness (Chu AYT, 2002). In the following chapters we will go through an analysis of proposed new beam types and their properties with respect to the requirements of the smallest possible stress under load and the smallest possible weight.

2. Materials & Methods

The study focused on the strength analysis of different wing beam is divided into two basic groups. In both cases the beams are the H-profile, but the changes are in additional elements, ribs or in the cross-section shape of the beams. All designs are based on the basic proposal, which shape and dimensions in millimetres are below in the figure 4. Total length of beams is 1500 mm.

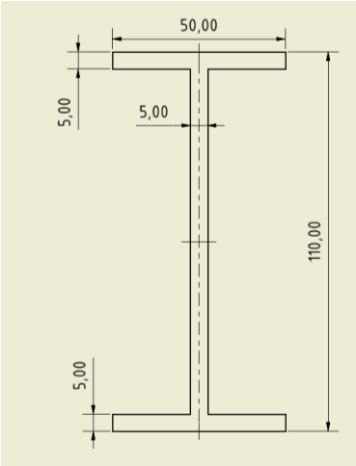

Figure 13: Cross-section dimensions of basic beam for numerical simulations. Source: Authors.

The material of the simulated beams is the Aluminium 6061 „Dural“ with common use in the aviation industry. During the simulations the beams were fixed at one of the ends and loaded with a steady force with different values on the upper beam flange. In the first group of beams were those that were supplemented by ribbing. The following figure 5 shows the first group. From top to bottom goes first the ordinary beam with the dimensions according to the figure 4, followed by the beam with transverse ribbing, the beam with ribs at an angle of 45 ° to each other and the last beam with parallel ribbing at an angle of 45 °.

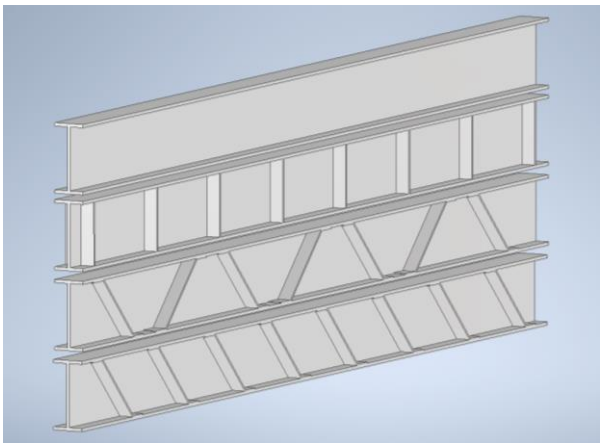

Figure 14: Group of tested beams with additional ribbing. Source: Authors.

Taking into account, the properties of the neutral axis and the danger of deformation of the beam wall, the authors investigated the modifications by additional elements with creating different cross-sections. The following Figure 6 shows the types of the beams that were examined.

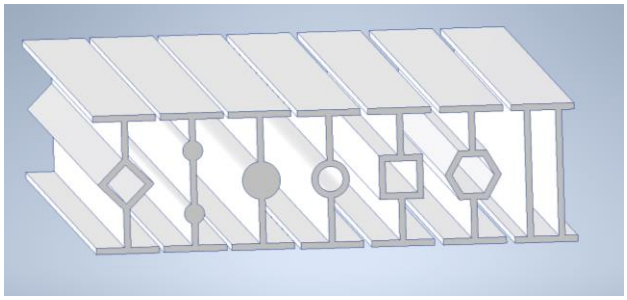

Figure 15: Cross-section patterns used for numerical simulations (from left to right – diamond, full dual „o“, full „o“, hollow „o“, rectangular, hexagonal, dual beam. Source: Authors.

The figure 6 Cross-section patterns used for numerical simulations (from left to right – diamond, full dual „o“, full „o“, hollow „o“, rectangular, hexagonal, dual beam

The numerical analysis was divided into a total of 16 parts and 4 different loads were applied for each beam type, which were graduated from 200 N, 400 N, 600 N to 800 N. The load was applied perpendicular to the top of the beam as shown in the figure 7.

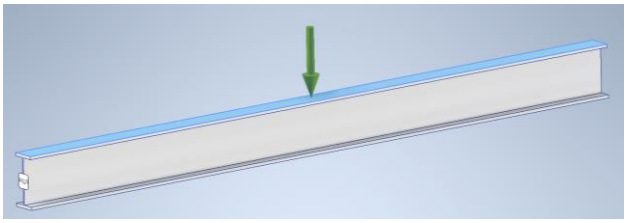

Figure 16: Beam attachment and direction and distribution of the applied force. Source: Authors.

The figure 7 Beam attachment and direction and distribution of the applied force

The results of numerical simulations were evaluated from three different points of view. These were the Von Mises Stresses (MPa), displacements (mm) and the weight (kg) of the currently simulated beam. The simulations were performed with Autodesk Inventor 2020 software using the strength analysis function. The average size of the element (as a length fraction of the bounding polygon) at network formation was 0.5. As already mentioned, the material in the simulations was chosen aluminium with the designation 6061, also known as “Dural”. An overall view of the basic beam simulation is shown in the figure 8.

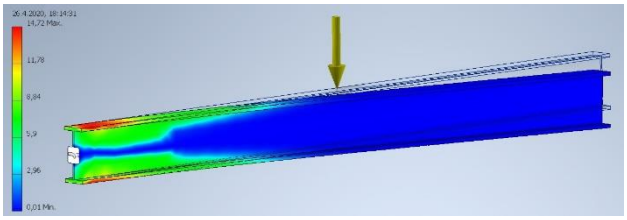

Figure 17: A view of the basic beam bending simulation with the course of Von Mises Stress (MPa). Source: Authors.

3. Results

The results of the simulations are shown in Table 1. From this table it is clear that when comparing the weight, the first group of beams was lighter than the second group. From the point of view of displacement evaluation and internal stresses, however, the results were opposite. The computational simulations show (Table 1) that the best rated beams include “dual beam” and “full dual “o””. For this reason, the team of authors focused on further monitoring the properties of these beams by their combination or dimensional modification, while maintaining a weight of approximately 5 kilograms.

Table 2: Numerical simulation results of beam designs. Source: Authors.

Beam	Max. Displacement 200N (mm)	Max. Tension 200N (Mpa)	Max. Displacement 400N (mm)	Max. Tension 400N (Mpa)	Max. Displacement 600N (mm)	Max. Tension 600N (Mpa)	Max. Displacement 800N (mm)	Max. Tension 800N (Mpa)	Weight (kg)
Additional Ribs									
No Ribs	0,691	4,986	1,384	9,972	2,076	14,96	2,767	19,94	4,05
Cross Ribs	0,685	4,715	1,37	9,43	2,055	14,15	2,74	18,86	4,342
Inclined opposite Ribs 45°	0,617	5,185	1,342	10,37	2,013	15,56	2,684	20,74	4,485
Inclined Parallel Ribs 45°	0,67	6,028	1,34	12,05	2,01	18,08	2,68	24,11	4,548
Profile Change									
Dual Beam	0,557	3,898	1,115	7,796	1,672	11,69	2,229	15,59	6,075
Hollow "O"	0,6863	5,094	1,373	10,19	2,059	15,28	2,745	20,38	5,036
Full "O"	0,678	4,847	1,356	9,692	2,035	14,54	2,713	19,39	6,308
Full dual "O"	0,636	4,72	1,272	9,439	1,908	14,16	2,544	18,88	5,041
Rectangular	0,663	4,755	1,326	9,509	1,989	14,26	2,652	19,02	5,771
Diamond	0,671	4,842	1,354	9,683	2,031	14,52	2,709	19,37	5,362
Hexagonal	0,664	4,78	1,328	9,559	1,992	14,34	2,656	19,12	5,644

Through gradual analysis, we came to the fact that the direct displacement of the elements closer to the flanges affects the overall rate of stresses and displacements under load. The final proposal (Figure 9(b)) is designed so that the “o” elements are shifted to the closest possible distance to the flanges, therefore 43 mm from the centre of the beam. This distance was chosen because of the space for the placement of the structure welds. In addition to this design, another model was investigated with the ribs addition perpendicular to the beam wall (Figure 9(a)).

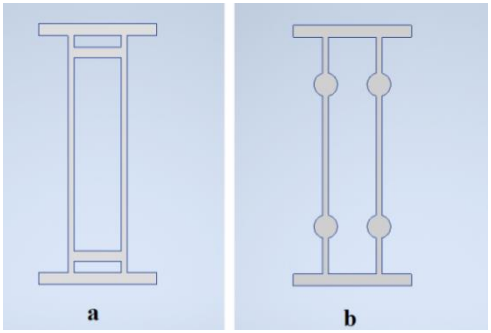

Figure 18: Visualization of improved and final beam designs - Dual Beam (half thickness) + middle ribs 43mm from center (a), Dual Beam (half thickness) + dual full "O" 43mm from center (b). Source: Authros.

The following Table 2 evaluates the numerical simulations of the additional designs. The final designs from the figure 9 are in the penultimate and last place in Table 2.

Table 3. Numerical simulation results of additional beam designs. Source: Authors.

Beam	Max. Displacement 200N (mm)	Max. Tension 200N (Mpa)	Max. Displacement 400N (mm)	Max. Tension 400N (Mpa)	Max. Displacement 600N (mm)	Max. Tension 600N (Mpa)	Max. Displacement 800N (mm)	Max. Tension 800N (Mpa)	Weigh t (kg)
Dual Beam (half thickness)	0,69	4,634	1,381	9,268	2,072	13,09	2,763	18,54	4,05
Dual Beam (half thickness) + dual full "O"	0,643	4,747	1,326	10,05	1,93	14,26	2,574	18,99	4,922
Dual Beam (half thickness) + dual full "O" 30mm from center	0,624	4,652	1,25	9,302	1,875	13,96	2,499	18,69	4,922
Dual Beam (half thickness) + dual full "O" 43mm from center	0,576	4,276	1,135	8,553	1,703	12,83	2,27	17,11	4,922
Dual Beam (half thickness) + middle ribs 43mm from center	0,583	4,035	1,168	8,071	1,752	12,11	2,336	16,14	4,779

It is obvious from the design that the additional ribbing and elements influenced the stress distribution in the materials. From the figure 10 (top) it can be determined that the design "Dual Beam (half thickness) + middle ribs 43 mm from centre" has a more even distribution of the stresses across the cross-section. In the proposal "Dual Beam (half thickness) + dual full" O "43 mm from centre" are the stress and forces carried by extra "O" elements in the cross-section. Authors also created combinations of the designs, but numerical simulations did not show significant improvements over the original designs

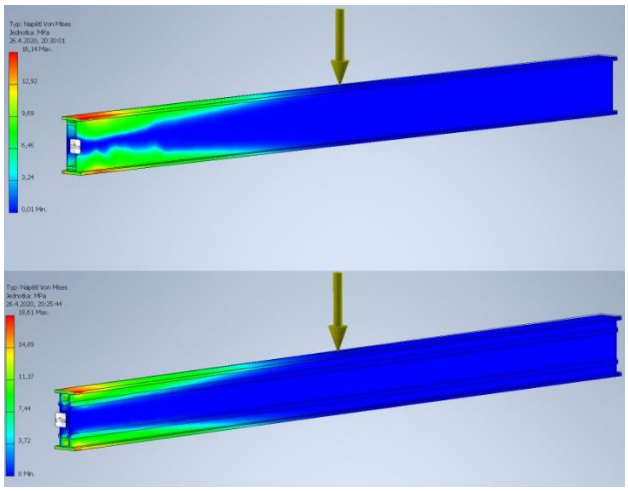

Figure 19: Visualization of the final beam designs with a distributed 800 N load. Dual Beam (half thickness) + middle ribs 43 mm from centre (upper part), Dual Beam (half thickness) + dual full "O" 43 mm from centre (lower part). Source: Authors.

The overview of selected design results is shown in the Graph 1, which contains proposals from Tables 1 and 2. The designs in the Graph 1 are numbered in ascending order from Table 1 (1-11) and Table 2 (12-16). From Graph 1 it is clear that the best strength characteristics has the design no. 5, i.e. "Dual Beam". Nevertheless, this beam has 16% more weight than the rest. For this reason, this design is inappropriate. From this point of view, however, it is necessary to consider the overall behaviour and susceptibility to fatigue and cracks (Čerňan, 2019).

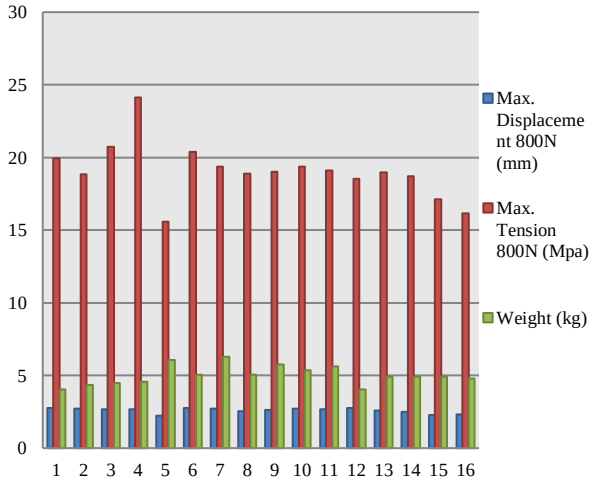

Graph 1: Comparison of Max. Displacement (mm) and Max. Tension (MPa) under 800 N load beside of total weight of beams. Source: Authors.

From the comparison of the other beams, the final properties from the figure 9 had the best properties. Therefore, these proposals were evaluated for further research and experimental validation. In addition to the designs, it is necessary to take into account the possibility of corrosion (Janovec, 2020) and fatigue wear. (Čerňan, 2018) In particular, wall thickness is prone to dimensional changes due to corrosion and cracks. However, the use of modern NDT diagnostic methods solves this problem (Janovec, 2019).

4. Conclusion

The study of the beam numerical simulations was focused on the design possibilities of increasing the wing structure strength. By performed simulations, it was possible to determine the beams with the best results, and subsequently to modify and optimize these designs. The study result are two designs of the H-profile with the double wall and additional elements as shown in the Table 2 and the Graph 1. Current designs are still the subject of research and appropriate optimization for further research. The given results can be experimentally verified and thus prove the correctness of numerical simulations. During the design process, the authors also tried to take into account the production technology of the given beams and the proposed designs to meet sufficient criteria for fast and efficient construction. In the case of the successful experimental verification, these optimized beams would be suitable in the wing construction use and could be considered to be used also in civil engineering, where the inspiration came from.

Acknowledgment

This work was supported under the project of Operational Programme Integrated Infrastructure: *Research and development of contactless methods for obtaining geospatial data for forest monitoring to improve forest management and enhance forest protection*, **ITMS code 313011V465**. The project is co-funding by European Regional Development Fund.

References

Abdel-Ghaffar, M.M.E., April 2003, "Limit-Load Analysis vs. Destruction Testing of Perforated Cold Formed Steel Cable Trays", 10th International Colloquium on Structural and Geotechnical Eng., Ain-Shams Univ., Egypt, ST02, pp.1-12.

Beňo, L., Bugaj, M., & Novák, A. 2005. Application of RCM principles in the air operations. Komunikacie, 7(2), 20-24.

Čerňan, J., Janovec, M., Hocko, M., Cúttová, M., 2018. Damages of RD-33 Engine Gas Turbine and their Causes. Transportation Research Procedia 35, 200–208. https://doi.org/10.1016/j.trpro.2018.12.028

Čerňan, J., Semrád, K., Draganová, K., Cúttová, M., 2019. Fatigue stress analysis of the DV-2 engine turbine disk. Aircraft Engineering and Aerospace Technology 91, 708–716. https://doi.org/10.1108/aeat-03-2018-0096

Chen, C.-C., Sudibyo, T., 2018. Effect of Intermediate Stiffeners on the Behaviors of Partially Concrete Encased Steel

Beams. Advances in Civil Engineering 2018, 1–15. https://doi.org/10.1155/2018/8672357

Chu AYT, Chan SL, Chung KF., 2002, “Stability of modular steel scaffolding systems - theory and verification. Proceedings of International Conference Advances in Building Technology Hong Kong”.

Janovec, M., Čerňan, J., & Škultéty, F. (2020). Use of non-destructive eddy current technique to detect simulated corrosion of aircraft structures. Koroze a Ochrana Materialu, 64(2), 52–58. https://doi.org/10.2478/kom-2020-0008

Janovec, M., Smetana, M., Bugaj, M., 2019. Eddy Current Array Inspection of Zlin 142 Fuselage Riveted Joints. Transportation Research Procedia 40, 279–286. https://doi.org/10.1016/j.trpro.2019.07.042

R. Kindmann, R. Bergmann, L. G. Cajot, and J. B. Schleich, “Effect of reinforced concrete between the flanges of the steel profile of partially encased composite beams,” *Journal of Constructional Steel Research*, vol. 27, no. 1–3, pp. 107–122, 1993.

S. D. Nardin and A. L. H. C. Debs, “Study of partially encased steel composite beams with innovative position of stud bolts,” *Journal of Constructional Steel Research*, vol. 65, no. 2, pp. 342–350, 2009.

Starší, D., 2020. O Letadlech - Dušan Slavětínský Starší - Konstrukce Nosníku. [online] Slavetind.cz. Available at: <http://www.slavetind.cz/stavba/konstrukce/kridlo/Konstr_nosniku.aspx> [Accessed 2 May 2020]

https://doi.org/10.26552/aer.C.2020.2.3

EXPERIMENTAL STATE OF THRUST TESTING OF AIRCRAFT RECIPROCATING INTERNAL COMBUSTION ENGINE

Matúš Mrva
Air Transport Department
University of Zilina
Univerzitná 8215/1
010 26, Žilina
mattusmrva@gmail.com

Pavol Pecho
Air Transport Department
University of Zilina
Univerzitná 8215/1
010 26, Žilina
pavol.pecho@fpedas.uniza.sk

Michal Hrúz
Air Transport Department
University of Zilina
Univerzitná 8215/1
010 26, Žilina
michal.hruz@stud.uniza.sk

Iveta Škvareková
Air Transport Department
University of Zilina
Univerzitná 8215/1
010 26, Žilina
iveta.skvarekova@fpedas.uniza.sk

Martin Bugaj
Air Transport Department
University of Zilina
Univerzitná 8215/1
010 26, Žilina
martin.bugaj@fpedas.uniza.sk

Abstract

The project "Experimental State of Thrust Testing of Aircraft Reciprocating Internal Combustion Engine" is aimed at creating a complex measuring device in order to obtain selected characteristics and parameters of the engine using different types of propellers. In addition to the basic measured parameters such as. thrust, temperature, speed and fuel flow will be a state of the art to test the latest prototype propellers designed for aircraft models. After its construction, the experimental state will be used as a study aid for testing various types of conventional as well as currently developed propellers, engine characteristics and teaching of the whole equipment in the process of teaching, training of aircraft mechanics and for presentation purposes of the University of Žilina.

Keywords

aircraft engine, aircraft propeller, thrust test

1. Introduction

At present, simple experimental stands with insufficient sensor equipment are used in radio controlled (RC) aviation to measure thrust and engine parameters. If electronic systems are used, these devices are costly and therefore the designers resort only to a cheap, basic and often quite inaccurate variant of the production of a simple stool using a load cell (Kovář, 1962). At present, there is no similar and unique experimental state within the universities in the Czech Republic and Slovakia focused on aircraft technology for experimental measuring thrust testing characteristics of RC aircraft propellers, which gives the project uniqueness. Manufacturers of large propulsion units and propellers test their prototypes in test rooms that are financially unaffordable for the needs of the university (Beňo, 1985)). It is the use of a model combustion piston engine and propellers to the required scale that make it possible to imitate the conditions of large test rooms on campus for relatively small funds in the form of experimental measuring device. In addition to the design, it should be noted that the technologies themselves for monitoring the parameters of model engines and their use, whether in solving problems with new propeller prototypes or as a laboratory prototype designed for teaching and measurement exercises make the project unique.

1.1. Inovative solution

The creation of such a device could bring a financially inexpensive variant of the device for experimental measuring thrust testing of various types of engines, testing new types of propellers for the University of Žilina and at the same time serve as a teaching aid for students studying this field and increase learning efficiency and interest about field of study. In addition to the teaching process itself, the project would be a contribution to the certification of an aircraft maintenance technician under the "EASA Part 147" regulation, which will be an essential part of the Aircraft Maintenance Technology study field. Specifically, it would be category B1 - certifying maintenance technician for two subcategories. They are B1.2 - Aeroplanes with Piston Engines, B1.4 - Helicopters with Piston Engines. And at the same time category B2 - certifying maintenance technician for all types of aeroplanes. The possibility of designing a fully functional prototype to test the characteristics on a reduced scale and while maintaining the relevance of the outputs is the main essence of an innovative solution for research and study of current needs of construction and design of aircraft propellers.

2. Materials & Methods

The implementation of the design and construction of the device is expected to be implemented in three main phases of

the project schedule. According to the chronological point of view, we can divide them into:

- construction,
- software and electronic part,
- running-in, calibration and testing.

2.1. Construction

In this phase, we focused on the construction of the experimental prototype itself to measure the thrust characteristics, which must meet the given strength and static conditions. The prototype itself will be constructed from available iron semi-finished products using different types of profiles. We used steel semi-finished products of class STN 42 11,600 to construct the table on which the device will be mounted.

In project was used three general types of construction segments:

- quare profile 30x30x1000 mm,
- rectangular profile 50x20x700 mm,
- L - profile 30x30x800 mm.

After cutting the correct lengths of the individual profiles, were proceeded to join them using electrode welding. We welded a rectangular platform to the back of the basic structure of the table, which serves as a weight holder. After finishing the welding work, we continued with the surface treatment. The whole table was sprayed with black matt synthetic spray paint. After thorough drying, we sprayed three coats of matt synthetic varnish on the entire structure to protect against chemical damage from the exhaust gases (figure 1). Concrete was used for the production of the weight, which was embedded in the mold together with the half-cast holder.

Figure 20: Finished table, platform, and weights. Source: Authors.

After curing, the same surface treatment was applied as for the table construction, with the difference that a different shade of paint was used. The next part followed, namely the production and mounting of the movable platform to the table using a linear guide. The platform on which the internal combustion engine, electronic sensors, fuel and electrical system will be mounted was made of a steel plate which was reinforced with two steel semi-finished products of the type: square profile 10x10x250 mm. The same surface treatment followed as the weights. The platform and table were connected using the necessary screws and a linear guide consisting of a pair of supported bars dimensions 25x450mm and four carts for the type of bar. The connection had to be perfectly centered and fine-tuned to ensure a smooth operation.

Figure 21: Internal combustion engine DLA 64 with three-bladed propeller. Source: Authors.

We succeeded and therefore we were able to proceed with the installation of a combustion, two-stroke, two-cylinder engine brand DLA (figure 2) with a capacity of 64ccm (2DLA0064 - Engine DLA 64 ccm, 2020). Together with the electronic ignition, was attached it to the platform using a screw connection. The engine is attached to the platform via four pieces of silent-blocks. The 500 ml fuel tank is attached to the platform in the bed and secured with cable ties. To control the entire our experimental measuring thrust testing device, a 3D design of the remote control unit was created, which was printed using a 3D printer from ABS material.

2.2. software and electronic part

The controller controlling the entire our experimental measuring thrust testing device contains a throttle lever, which is connected via a Bowden cable to the engine carburetor throttle, electronic ignition supply battery, two alphanumeric displays, a series of switches and signaling LEDs, a potentiometer and an Arduino Mega ADK control unit. A complex ARDUINO microprocessor system was used to measure individual variables such as thrust, temperature and fuel consumption. The whole system consists of the following components used:

- Arduino MEGA ADK control unit,
- 2x Alphanumeric displays 20x4 with circuit PCF8574, (LCD Diplej, 2020)
- Flow meter BioTech FCH-m-POM-LC, (HAREENDRAN, 2020)
- 2x Pt100 temperature sensor, (Měření teploty pomocí Pt100, 2020)
- 2x HX711 module,
- Weight sensor, (Arduino Scale With 5kg Load Cell and HX711 Amplifier, 2020)

- Wiring,
- DC source.

The individual sensors were placed on the platform and specific points so as to ensure the most reliable measurement and protection against vibrations. The software part consisted of designing and developing a simple code with which the control unit could perform individual measurements. The code was created in the Arduino IDE program, which works with the Wiring environment. After the successful installation of all sensors and the upload of the created program to the control unit, the completion of the entire electronic part followed, the connection of the electronic circuit and the preventive test of all sensor parts. (Čtení dat z arduina a ukladání dat do PC, 2020)

2.3. Running-in, Calibration and Testing

After these operations, the experimental measuring thrust testing device was theoretically completely finished. In practice, it was necessary to run the internal combustion engine first, before the measurement itself.

Figure 22: Engine run-in DLA 64. Source: Authors

During the run-in, all instructions from the engine manufacturer, DLA, were followed. Specifically, it was about adjusting the combustion mixture, the correct procedures for the initial setting of the carburetor and its subsequent tuning, the use of the specified propeller size and engine speed control. (Nový motor, 2020) After the successful start-up of the engine, the individual sensors were calibrated using calculations of the components used and designed by us. These calculations were then correctly defined and tested by editing the code. After performing these measures, the testing of the entire our experimental measuring thrust testing device was started. This consists of the following steps:

1. Switching on the system: Switch No. 1 turn on the power supply of the Arduino, all sensors, the display (the display shows a welcome message / the name of the device), then the current temperature of both temperature sensors starts. Switching on the system is indicated by an LED diode and a switched on display.
2. Start the engine: Start the combustion engine - manually. (Authorized and trained teacher) Switch No. 2 turns on the ignition. Ignition on is indicated by a lit LED.
3. Warming up of the engine to the operating temperature: After starting the engine, waiting for the operating temperature of the engine, which we find out from the data on the display, which are still measured by temperature sensors.
4. Starting the measurement: After reaching the correct operating temperature of the engine, we start the measurement. We start this with switch No. 3, which will be a single-position reversible one. The start of the measurement will be indicated by an LED diode. The displays will show "Measurement", current engine thrust, fuel consumption and individual temperatures. The time (2-5min) will also be counted down, which will be divided into 5 sections according to which the engine speed will be added. E.g. 0-30s - 20% gas, 30-60s - 40% gas ...
5. End of measurement: After the end of the measurement time, the measurement is switched off with switch no.3. The measured values will be recorded by a connected laptop and in Microsoft Excel it will create graphs from individual measured quantities. The LED indicating the ongoing measurement goes out. At the end of the measurement, the throttle lever is set to idle speed position.
6. Switching off the system: The engine is switched off, then the ignition is switched off (the LED goes out) and finally the entire power supply of the system.

After a successful calibration and a series of tests, the latest imperfections have been fine-tuned. The device was prepared for operation, teaching, presentation and defense of the diploma thesis of the student Bc. Matúš Mrva.

3. Results

The project “Experimental state of thrust tests of aircraft piston internal combustion engine” will serve as a practical and at the same time theoretical part of the diploma thesis of the student Bc. Matúš Mrva. The resulting experimental state will consist of a prototype of a thrust characteristic measuring device, a combustion piston model engine with accessories for its operation and a series of test model propellers with different properties. After the end of the project, such an experimental state will serve, in addition to the research focus, mainly as a teaching aid for students dealing with the issue and for future aviation technicians. In addition to practical outputs, the project is also focused on the presentation of achieved results in publications at domestic and foreign conferences and magazines.

3.1. Project Benefits

3.1.1. Scientific addition

The main scientific contribution of this project is to bring a modern instrumental teaching aid that will use current technologies in the field. The task of this device will be to measure the selected parameters and properties of the engine

depending on the type of propeller used. Based on these data, it will then be possible to analyze specific modifications and modifications in the development and innovation of aircraft propellers. In the course Aircraft Propellers, students are acquainted with the current trend in the development of aerodynamic properties and materials used in aircraft propellers, with emphasis on reducing noise and increasing thrust efficiency while reducing overall aerodynamic drag. For these reasons, the Department of Air Transport is also focused on research and innovation in this area with material support through external manufacturers in the final work.

3.1.2. Addition for practice

We emphasize the simplicity and efficiency of the project, and the result of the project will be fully functional instrumentation that can be used to monitor various types of internal combustion piston engine parameters, based on which it will be possible to determine further procedures in the development of the tested propeller. In case of successful test results, the device is planned to be used as a practical teaching aid for students of the Department of Air Transport, especially for students of Aircraft powerplant, Aircraft Propellers and Maintenance Procedures 1 and 2. The device will be designed and constructed so that in the future modify its components, optimize it and integrate new installations. These include modifications to the use of other internal combustion engines, the addition of additional sensors or the updating of the program for the Arduino microcomputer unit. In terms of usability for direct practice, the project is focused on cooperation with aircraft manufacturers

model propellers, which could be measured in the future as part of joint research and processed in the form of final theses of students at the Department of Air Transport, respectively to verify the design and innovative designs of new types of propellers designed for civil aviation.

4. Conclusion

The aim of the article and the project was to construct a comprehensive device for aircraft engines, whose main task will be to monitor selected engine parameters with their subsequent analysis and use of this information for the purpose of modifications and design of new prototype propellers, whether for aircraft modeling or civil aviation. At the same time, the project will serve as a study aid within the teaching process, as well as in solving final and semester works. The whole device is made of easily accessible components and materials so that there is no problem with the availability of spare parts or modification for the use of another type of engine or configuration. This opens up new promising opportunities for various developments in the coming years. In conclusion, we can state that we were advised to build a functional experimental measuring thrust testing device that can measure the specified parameters using different types of propellers and engines and we can adequately evaluate and apply the measured quantities for different types of use.

Acknowledgement

The article is published as one of the outputs within the grant projects UNIZA Grant System - Call No. 2/2019

References

2DLA0064 - Motor DLA 64 ccm (dvouválec) včetně tlumiče a příslušenství, viewed 15 September 2020 [online: https://www.tatramodel.sk/zakladna-ponuka/spalovacie-motory/nahradne-diely/nahradne-diely-dla/2DLA0064-motor-dla-64-ccm-dvouvalec-vcetne-tlumice-a-prislusenstvi/]

Arduino Scale With 5kg Load Cell and HX711 Amplifier, viewed 21 September 2020 [online: https://www.instructables.com/Arduino-Scale-With-5kg-Load-Cell-and-HX711-Amplifi/?fbclid=IwAR0m_un_7ReagvY1SoH2oQV9jGDpMMY2sz3iTFMjVxHMlnTs8MH5sDm8fzg]

BEŇO, L., Letouny a jejich systémy: Vrtulové pohonné jednotky s pístovými motory. 1985. Bratislava: VIDEOPRESS

Čtení dat z arduina a ukladání dat do PC, viewed 21 September 2020 [online: https://arduinoprojekt.webnode.cz/news/cteni-dat-z-arduina-a-ukladani-dat-do-pc/]

HAREENDRAN. T.K., Working with Water Flow Sensors & Arduino, viewed 20 September 2020 [online: https://www.electroschematics.com/working-with-water-flow-sensors-arduino/?fbclid=IwAR3K-L9xYE7reIAd1qo7SAwBpRS2nEmjokUAnL-TkbFMgc2TOhydFLKlJOc]

KOVÁŘ, R., Zkoušení leteckých motorů. [s.l.], 1962. 387 s. Skriptum. Vojenská

LCD Displej, viewed 20 September 2020 [online: https://navody.arduino-shop.cz/zaciname-s-arduinem/lcd-displej.html]

Měření teploty pomocí Pt100, viewed 21 September 2020 [online: https://navody.arduino-shop.cz/arduino-projekty/mereni-teploty-pomoci-pt100.html]

Nový motor, viewed 14 September 2020 [online: http://www.kolmanl.info/index.php?show=smotory_nove#smotory_nove_uv]

https://doi.org/10.26552/aer.C.2020.2.4

SPACE FLIGHTS A NEW OPTION FOR INTERCONTINETAL TRAVEL – SOLUTION DESING

Dominik Mrňa
Air Transport Department
University of Žilina
Univerzitná 8215/1
010 26, Žilina
dominik.mrna@stud.uniza.sk

Abstract

This paper describes problem of space flight intercontinental flight with passengers or cargo via suborbital orbits. It describes the necessary monitoring network as well as the operating procedures with connection of flights in airspace and in space itself. Paper takes into account existing models of spacecraft (space vessels) and concept designs to introduce possible solutions to this type of travelling. Last section deals with the issue of ground infrastructure – spaceport, for a given type of transport and focuses on the existing spaceport in USA and presents it as a model for future spaceports around the world.

Keywords

space flights, spacecraft, monitoring, spaceport

1. Introduction

Nowadays, a lot of start-up companies which would like to use space, in particular altitude above 100 kilometres, which represents the imaginary boundary between airspace and space (Zahari, Romli, 2019), for flights between continents with passengers or cargo. International legislation about the use of space allows to each country use space for socio-economic purposes with condition that space will be used only for peaceful purposes (Outer Space Treaty, 1967). Some companies, mainly in the USA, have started operating aircraft for space tourism. Some of these companies would like to start intercontinental flights in future. This technology would significantly speed up connections between destinations. Most of long-distance flights would be completed in less than half an hour (Musk, 2017).

Many subsystems will be needed for the whole system to work smoothly without problems. Advantage is that a similar system is using for the needs of satellite operations. Therefore, certain procedures could be implemented, and certain devices could be applied to the space travel segment.

2. Methodology

The used methodology consists in introducing basic components for traveling in suborbital orbits around the Earth. The gradual development of concepts, physical equipment and infrastructure seems to be suitable for updating the proposed concepts in the past. Content of this paper is presentation of the possibilities for surveillance and monitoring networks, means of transport and ground infrastructure.

2.1. Surveillance network and monitoring

To ensure safety environment, a new surveillance network will be needed to ensure tracking and surveillance of spacecraft during space flight. Operators have to take into account surveillance and tracking network for flight phase in airspace. For these purposes, operators or navigation providers could use existing surveillance network for aviation. Data sharing within these two spaces will be needed. Air traffic control would ensure control and safety in airspace and new centres of space traffic control would ensure control and safety of space. Experts in the field suggest a transition Flight Level of 650, circa 22 kilometres. In case of economic efficiency, space navigation providers could use a surveillance network from Space Traffic Management system, which is used for monitoring and tracking of objects for collision warnings of satellites. Nowadays, USA owns the most developed surveillance system called Space Surveillance Network (SNN), which is displayed in Figure 1. This system consists from ground based and space radars with 3 types of sensors placed around the world. Space-based sensors are not included in Figure 1.

Composition of the SSN system:

1. Conventional radars,
2. Phase-array radars,
3. Electro-optical sensors GEODSS (Ground-Based Electro-Optical Deep Space Surveillance),
4. The Midcourse Space Experiment (Sgobba, Allahdadi, 2013).

Figure 23: Location of all ground based sensor of SSN. Source: https://www.economist.com/briefing/2019/07/18/attacking-satellites-is-increasingly-attractive-and-dangerous

Hovewer extensive and developed this system is, it is not perfect and cannot predict the exact objects locations during a conjunction. As a result, there is a predicted location for each object. Reality is that object could actually be anywhere within an oblong bubble surrounding that predicted location (Peterson et al., 2018). It means that tracking object has many possible positions around the actual/real position. The bigger this bubble is, more false alarms of crash are produced. At present, experts in the field are trying to minimise this bubble to the smallest possible size by the ideas how to minimise the future population growth or by improved/additional data and processing (Peterson et al., 2018).

2.1.1. CNS

If we take into account the CNS – Communication, Navigation and Surveillance, the communication segment would be identical to the current concept and procedures. It means, that participants could use standard radio communication or digital communication (Tullmann et al., 2017).

Navigation would need to be standardised for space travel and similar to today's RNP (Required Navigation Performance) used in air transport is recommended. It is expressed by the distance to the intended position that an aircraft must comply with in at least 95% of the total flight time (Tullmann et al., 2017). Based on the navigation accuracy of spacecraft equipment and on the manoeuvrability of this vehicle, separation standards in airspace and space will be established. Operators have to take into account that certain concepts of spacecraft, especially those with limited manoeuvrability (rockets). Those will be not fully integrated into airspace, as concepts with horizontal take-off and landing.

RNP only applies to airspace, specifically to FL650. As others physical laws apply in space, it will be necessary to develop new navigations systems and its standards. New space vehicle would have to use two different navigation systems. This navigation system designed for the space environment could take the example and best practices from the operations of the Space shuttle. According to the technical specifications given in the NSTS New reference manual (1988)[a], Space shuttle navigation system was composed of three inertial measurement units, three tactical air navigation units, two air data probe assemblies, three microwave scan beam landing systems and two radar altimeters. For a detailed example, this system consisted of inertial measurement units, star trackers, crewman optical alignment sight, TACAN, air data system, microwave scan beam landing system, radar altimeter, accelerometer assemblies and orbiter gyro assemblies. Solid rocket booster rate gyro assemblies were used for navigation during launch.

For the proper function of surveillance, a concept should combine the data from sensors and radars used to monitor air traffic and space traffic on orbits. When the spacecraft will pass a FL650, it will be necessary to ensure a smooth transition of data between networks and equipment for air traffic and space traffic monitoring. Spacecraft should use a ADS – Automatic Dependent Surveillance, when the target itself determines its position and send information about it to the ground systems (Novák, 2010). FL650 ~ 60000 feet is selected as the boundary where responsibility passes from the area of air traffic control to the area of space traffic control. This transition boundary is also chosen mainly because most of surveillance aviation systems are limited to this altitude (Tullmann et al., 2017).

2.1.2. Space traffic control

For needs of space flights, it would be necessary to create space flight control centers. Controllers would be responsible for safety and flight above the FL650. Cooperation with air traffic control will be also necessary because some segments (departure, arrival) of flight will take place in airspace. To establish rules and procedures for transferring flight from airspace to space and vice versa, the usual procedures of a flight between individual FIRs could be used. In this case, a point at which will be flight transferred is precisely defined. This should include the transmission of flight data between traffic control units via online interfaces – principle of OLDI. Some sources state that STCO should also be responsible for movements at the spaceport. However, this depends on used aircraft (spacecraft) concept.

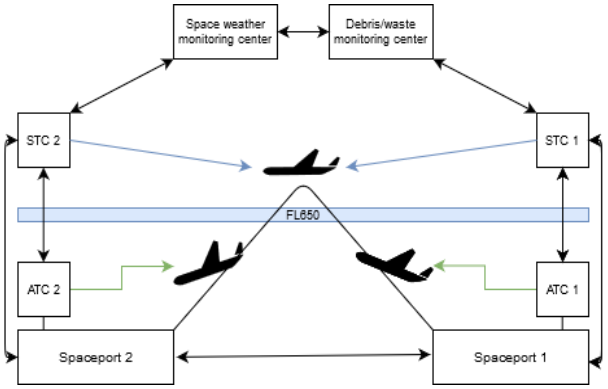

Figure 24: Diagram showing the connection of individual elements involved in space flights.

From text above and Figure 2, we can assume that air traffic controllers will continue to control of spacecraft during departure and arrival segment of flight in airspace. These steps will add new responsibilities, and therefore in case of future space operations, training should be added.

2.1.3. Monitoring centers

Besides of monitoring of the spacecraft and other space vehicles in orbit, it will be also necessary to monitor space waste or debris around Earth and monitor the state of space weather. According to NASA (2017), orbital debris is any man-made object in orbit around the Earth which no longer serves a

useful function. Such debris includes nonfunctional spacecraft, abandoned launch vehicle stages, mission-related debris and fragmentation debris. According to ESA (2020) statistic, number of functioning satellites is about 3000 and number of tracked debris objects is about 27370. According to NASA (2021), the highest density of debris is between 800 and 850 kilometers. Referring to Tullmann (2017), the maximum altitude of a hypothetic flight could be 500 kilometers. Figure 3 from Lucken, Hubert and Giolito (2017) shows the density of space debris and waste at different altitudes.

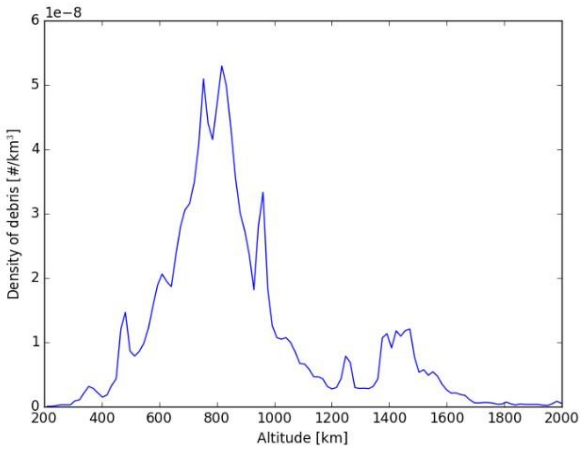

Figure 3: Density of debris at different altitudes. Source: Lucken, Hubert and Giolito (2017).

The attached graph in Figure 3 shows that the density of space debris up to 500 kilometers is not very high. However, there is still a risk of a possible collision. Based on the known trajectory between the destinations and based on the performance parameters of the spacecraft, it would be possible to calculate distances between the spacecraft and the space debris or satellite for each second of flight. The NORAD Two-Line Element database seems to be suitable for these needs. It contains trajectories of all monitored objects. Flight planning center in cooperation with debris monitoring center should verify risk of collision during whole flight. In case of possible conjunction with other objects, slot of departure time will be released to avoid a potentially dangerous situation. This means that the distance which poses a danger to the vehicle has to be introduced. In case of ongoing flight, updated informations (in form of bulletin) with possible conjunction and correction maneuvers should be presented to crew by space traffic controller (Figure 4).

State of Space weather and its forecasting is very important for operation. The National Oceanic and Atmospheric Administration's (NOAAA) Space Weather Forecast Center has sufficient monitoring and forecasting capacity. NOAAA can provide information about space weather conditions, where data from the last observation and thus predictive models are given. These warnings apply to geomagnetic storms, solar storms, and radio blackouts.

The state of space weather around the Earth is influenced mainly by the Sun. Mainly by the coronal mass ejection, solar flares, extreme ultraviolet radiation (EUV) and many others. Radiation caused by solar radiation storm from coronal mass ejection are dangerous because it has impact mainly on human health. EUV and solar flares mainly affect the ionosphere. This is mainly ionization, when the so-called radio blackout can occur, i.e., the loss and impossibility of a radio connection. The highly ionized atmosphere also causes an increase of drag as the ionosphere becomes denser. Therefore, orbiting devices must perform frequent correction maneuvers to return to their original orbits (NOAAA, 2021). NOAAA constantly monitors the state of the Sun and its accompanying phenomena. For space flight operations is NOAAA able to issue forecasts or warnings in advance.

In case of severe conditions, flight planning center in cooperation with NOAAA or equivalent space weather monitoring center should be able to issue warnings of these phenomena or suspend operations. Just because of the loss of communication, such a flight poses a serious safety problem. As some phenomena can last from hours to days, it is not considered logical to issue slot time. In the event that a sudden incident affects an ongoing flight, it will be necessary to issue safety procedures and guidelines for this purpose.

The above-mentioned centers already exist mainly for the satellite operations, they could potentially expand their capacities and capabilities for needs of space point-to-point flights and achieve better cost-effectiveness.

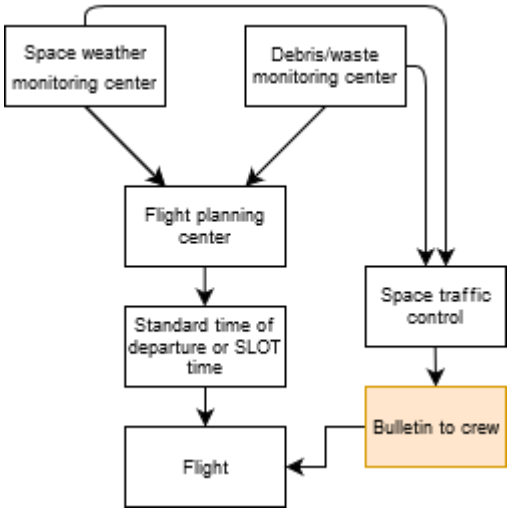

Figure 4: Flight planning scheme.

2.2. Spacecraft for suborbital flight

Today, experts are working with three main concepts of spacecraft for suborbital flight. These concepts are:

1. Vertical take-off and landing
2. Horizontal take-off and landing,
3. Hybrid take-off and landing.

2.2.1. Vertical take-off and landing

This concept works with conventional rockets launch from Earth. Main difference from standard rocket is, that this type is fully reusable, because first stages are driven back to Earth. This leads to economic efficiency, because costs for launch are smaller than in case of disposable rockets.

SpaceX's Starship rocket (Figure 4) represents the appropriate model of this concept. This ship is mainly designed for Mars's mission and satellites launching operations, but SpaceX takes into account a possibility of Earth-to-Earth traveling (Musk, 2017). Elon Musk, CEO of SpaceX, said that average price of ticket for suborbital intercontinental flight will be about 1200 USD/flight (Dinkin, 2017). Connection time between two destinations, depends on distance is estimated about 25 – 40 minutes. Given such a price, there could be considerable demand for such travel, as experience in space tourism shows that, due to the significant cost of orbiting the Earth, orbital space tourism will not be affordable for the general public in the coming decades (Yi-Wei Chang, 2020).

Figure 5: Big Falcon Rocket with Starship module. Source: Musk, 2017.

2.2.2. Horizontal take-off and landing

In the future, this type of spacecraft could use the experimental engine SABRE (Synergetic Air Breathing Rocket Engine), which in the initial flight phase works as conventional jet engine with additional combustion and after reaching a certain altitude, the principle of engine operation changes to rocket engine. This engine was originally designed for the British concept of the HOTOL (Horizontal take-off and landing) spacecraft from the 80s.

A newer concept that would use SABRE engine is also from Britain and is called Skylon Spaceplane (Figure 5). This spacecraft would be able to accelerate to Mach 5.5 when reaching an altitude of 28 kilometers. Above this altitude up to 90 kilometers, rocket engine would be able to accelerate Skylon to Mach 27.8 (Hempsell et al., 2014). Unfortunately, this concept is currently only on blueprints a there is only an engine, which is currently in the testing phase. From available data and operating manuals, we know that this type of spacecraft would need a special RWY only for Skylon, approximately 5.5 kilometers long (Hempsell et al., 2014).

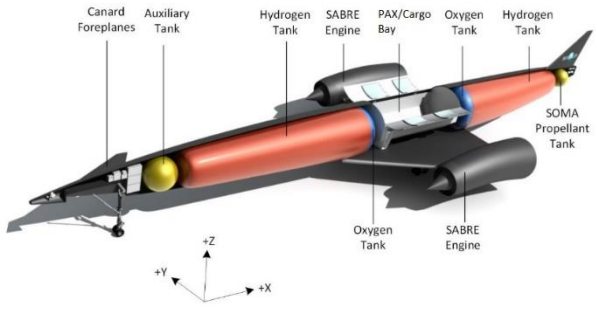

Figure 6: Model of Skylon Spaceplane with interior equipment. Source: Hempsell et al.,2014.

This concept is designed for the transport of passengers and cargo, where replaceable containers for cargo or passengers would be installed in the aircraft as required. In the case of PAX version, a container would be able to carry 24 passengers and 7800 kilograms of cargo. Container with satellite deploying mechanism (satellite up to 10 tons) is another option (Hempsell et al., 2014). Passenger container is designed with full life support systems, so no spacesuits would be needed.

In addition to this concept (Skylon), European Union has been working on the FAST20XX project, which has explored two new concepts of suborbital means of transport. The first of these is the Alpha, a small space vehicle with a hybrid launch principle. The second project is SpaceLiner, a two-stage rocket (Starship principle). However, this second concept was not considered feasible until the second half of the 21st century (Mason-Zwaan, Moro-Aguilar, 2013).

2.2.3. Hybrid take-off and landing

As a last option, we chose the already existing spacecraft of the American company Virgin Galactic called VSS Unity/Space Ship Two. This company does not currently use its spacecraft for suborbital point-to-point traveling but only for space tourism purposes. The company has also signaled its interest in leveraging its space technology to develop high-speed, point-to-point travel (Grush, 2020). We chose this company as an appropriate example, because it shows a feasible option to launch spacecraft into space, albeit on a small scale.

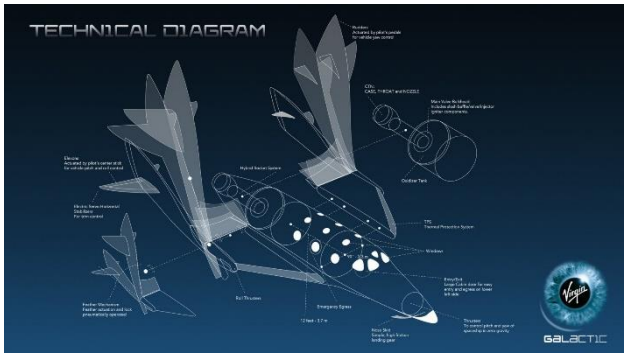

Figure 7: Technical diagram of VSS Unity Spacecraft. Source: https://www.virgingalactic.com/learn/

The whole mission is to bring the VSS Unity spacecraft to space by the mother aircraft (mobile launch pad) VSS Eve. It takes-off as a conventional aircraft and bring the VSS Unity to a height of 45000 – 50000 feet (13.7 – 15.2 kilometers), where it will come to disengage and ignite the rocket engine, which will get the spacecraft to the edge of space. So far, the height has reached 80 kilometers (Karman's border in the USA), but in the future Virgin Galactic wants to reach a limit of 110 kilometers. After reaching the highest point, the spacecraft will return to its home base in New Mexico using a gliding flight. The spacecraft is designed for 2 pilots and 6 passengers. (Sheetz, 2020).

According to available sources, the company has made a partnership with NASA to work together to develop a high-speed aircraft capable of intercontinental ballistic flight around the Earth. For this development, the company wants to draw on its experience in the design and operation of the aforementioned spacecraft (Etherington, 2020).

2.2.4. *Maneuverability of vehicle*

The maneuverability of an aircraft also needs to be addressed. For concepts with hybrid and horizontal take-off, movement in the atmosphere around the main axes will be provided via movable control surfaces. Rocket during launch uses thrust vectoring for basic maneuvering. In space, special system for maneuvering the vehicle will need. The aircraft could therefore use the reaction control system (RCS), which is also known from the operation of space shuttles and other space vehicles. This RCS or orbital maneuvering system provides the thrust for orbit insertion, orbit circularization, orbit transfer, deorbit, abort to orbit (NSTS News reference manual, 1988)[b].

2.3. Spaceports

New airports/spaceports will be needed to operate spacecraft and other space vessels and vehicles. Some research recommends/suggests that the construction of such spaceports be carried out as an extension of some of the world's hubs for air transport, in order to copy routes between those destinations (Tullmann, 2017). But experiences show that even the usual expansion of the airport seems to be very problematic. Such extension is only possible if a hybrid or horizontal spacecraft concept is used for the flights. In case of vehicles with vertical take-off, existing cosmodromes could be used, or new ones could be built in order to copy routes. In addition, the ground infrastructure should include fuel storage areas in accordance with applicable regulations, a fire extinguishing system suitable for the planned activities. In the first instance, such a place must contain hangars of the correct size with adequate dimensions to accommodate vehicles and to allow all necessary activities there before and after the flight or during the turnaround between flights (Santoro et al., 2018).

At least the basic infrastructure already exists in America for these flights and vehicles. For example, Spaceport America in New Mexico, which uses Virgin Galactic for its needs. Unfortunately, there is no similar spaceport in Europe and no spaceport has been built to launch rockets. For these purposes, ESA uses spaceport Kourou located in French Guaina (ESA, 2020).

Figure 8 shows, that spaceport object does not differ significantly from a regular airport. It is equipped with a passenger check-in terminal and apron area. The terminal is also use as a hangar for aircraft storage and aircraft maintenance. Spaceport is equipped by concrete RWY with dimensions 3658x61 meters, with 16/34 orientation (Airnav.com, 2020). Spaceport also has access to Special Airspace Restricted Areas – 5111A and 5111B, which do not have an upper limit on request. (FAA, 2020)

Based on official data, this spaceport is able to provide the following services:

1. Horizontal launch and landing,
2. Suborbital flight training and research,
3. Weightless flights,
4. Test-flight aviation,
5. Straight-line aerodynamics testing,
6. Unmanned flights (Spaceport America, 2020).

In addition to the RWY, Spaceport also has facilities and infrastructure for rocket launches. Company is also adding a new infrastructure for Vertical Launch. These improvements are expected to be finished by mid-2021 (Spaceport America, 2020).

Spaceport America clearly shows to us that several types of space vessels can be served in one special place. Therefore, this possibility should be considered in future planning and that instead of costly construction of individual space vessels launch facilities (rockets – cosmodromes, spacecraft – spaceports), combined solutions could be built.

Figure 8: Spaceport America, New Mexico from satellite image. Source: Google Maps

3. Results and discussion

At present, we can only rely on solutions proposals that deal with the topic, because point-to-point travel on suborbital path is unfortunately not used today, or not practice at all. The first physical facilities are under construction or are in operation mainly in the United States, where flights are performed only to a minimal extent.

The similarities with air transport and satellite operations may seem to be an advantage in connection with the creation of rules and standards for operation. This new concept could work with the know-how and best practices from these segments. It is necessary to mention that the existing monitoring (communication) networks could be used, especially in the initial stages, to avoid an excessive increase in the cost when building new networks. We assume that initial operation will be not so burdensome for the system.

The SpaceX with its Starship rocket, seeks to connect destinations on the planet through suborbital flights. The first tests of this rocket are currently underway. This rocket has many uses. From our point of view, it seems that the company focuses more on getting astronauts to Mars with the aforementioned rocket than on the possibility of traveling Earth-to-Earth. Getting people to Mars have more potential and greater prestige. Referring to information from official Elon Musk's Twitter account, prediction of the first test flight of the Starship into space could take place by 2022 – 2023.

Virgin Galactic is currently in the process of launching its first flight with passengers. However, form the already mentioned

alliance with the American NASA, there is no exact date when the first flight of the newly developed supersonic aircraft should take place. Given the current situation of the sets, is assumed that the creation of an aircraft will be not a priority for those companies. But concept of mobile launch pad for possible suborbital traveling looks like the right, because by using a mobile launch pad (VSS Eve) spacecraft consumes less propellant than an equivalent ground-launched vessel and is more sustainable and cost-effective (Cordis EU research results, 2015).

Europe would also like to have a share on the suborbital travel market. Unfortunately, we can work only with rough designs of Skylon concept or others. For Skylon spacecraft, the SABER engine is going to the test phase, so we do not yet know the overall results. From the available sources we know that developed precooler for this engine was able to successfully cool the system under conditions of air flow at the speed of Mach 5. It is making a significant milestone in the development of this engine (Reaction Engines, 2019), not only for this spacecraft.

As far as the safety of these devices is concerned, in addition to active elements, it proposes to include passive elements in the form of ballistic parachute systems. These parachutes would be fired in an emergency and the device itself would then descend safely to Earth (Škultéty, Čerňan, Rostáš, 2019).

As the FUA concept is being moved, especially in European region, in order to increase the efficient use of airspace (Eurocontrol, 2020), author considers the concepts of spacecraft with horizontal and hybrid take-off to be the most optimal choice, because using a rocket, it is still necessary to take into account its limited manoeuvrability and thus the need of own segregated airspace. In other concepts, the is a possibility, when spacecraft is able to achieve established navigation accuracy (RNP), full integration into the air transport system without the need of segregated/reserved airspaces.

For many concepts, we do not know the exact date when they should start operation, yet. At best, we know only a very rough estimate. It can be assumed that the crisis in air transport caused by the global pandemic of COVID-19 will significantly delay the dates already issued or it will completely suspend the development of flying space vessels.

In the end we state that vehicles and infrastructure are constantly being developed and improved. Therefore, current devices may seem outdated in the near future and may be better and improved than the models shown in this paper.

4. Conclusion

Suborbital travel offers many opportunities for the development of transport on Earth. The biggest advantage is of course, the speed of vehicle, because higher speeds can be achieved at high altitudes. Mainly due to the fact that sonic boom at higher altitudes is not a problem, but mainly due to the different composition of the atmosphere. This paper describes the most important elements that will be needed to perform this type of flights. It deals with the problem of monitoring networks for transport, which includes the actual monitoring of spacecraft as well as other objects on orbits and space weather. CNS, airport design and possible variants for spacecraft are also described. This paper applies to generally known matters and knowledge gained in the development and operation of existing facilities and infrastructures that would be suitable for this type of traveling.

5. References

AIRNAV.COM, 2020. *Spaceport America*. Available at: https://www.airnav.com/airport/9NM9 (Accessed 5 October 2020).

CORDIS EU research results, 2015. *Air Launch space Transportation using an Automated aircraft and an Innovative Rocket*. Available at: https://cordis.europa.eu/project/id/685963 (Accessed 7 October 2020).

Dinkin, S., 2017. *Estimating the cost of BFR*. Available at: https://www.thespacereview.com/article/3343/1 (Accessed 2 October 2020).

ESA, 2020. Space *Environment Statistics*. Available at: https://sdup.esoc.esa.int/discosweb/statistics/ (Accessed 1 October 2020).

ESA, 2020. *Europe's Spaceport.* Available at: http://www.esa.int/Enabling_Support/Space_Transportation/Europe_s_Spaceport/Europe_s_Spaceport2 (Accessed 5 October 2020).

Ethertington, D., 2020. *Virgin Galactic is partnering with NASA to develop supersonic point-to-point air travel*. Available at: https://techcrunch.com/2020/05/05/virgin-galactic-is-partnering-with-nasa-to-develop-supersonic-point-to-point-air-travel/?guccounter=1 (Accessed 2 October 2020).

EUROCONTROL, 2020. *Advanced flexible use of airspace*. Available at: https://www.eurocontrol.int/concept/advanced-flexible-use-airspace (Accessed 7 October 2020).

FAA, 2020. *Special use of airspace*. Available at: https://sua.faa.gov/sua/siteFrame.app (Accessed 5 October 2020).

Grush, L., 2020. *Virgin Galactic releases renders of proposed supersonic jet that can reach Mach 3*. Available at: https://www.theverge.com/2020/8/3/21352390/virgin-galactic-supersonic-aircraft-mach-3-rolls-royce (Accessed 2 October 2020)

Henpsell, M. et al., 2014. *SKYLON Users' Manual*. Available at: https://web.archive.org/web/20160328220308/http://www.reactionengines.co.uk/tech_docs/SKYLON_Users_Manual_Rev_2.1.pdf (Accessed 2 October 2020).

Lucken, R., Hubert, N., Giolito, D., 2017. *Systematic space debris collection using Cubesat constellation*. 7th European Conference for Aeronautics and Aerospace Sciences. DOI: 10.13009/EUCASS2017-678

Masson-Zwaan, T., Moro-Aguilar, R., 2013. Regulation private human suborbital flight at the international and European level: Tendencies and suggestions. Acta

Astrounautica 92, Issue 2. 243-254. https://doi.org/10.1016/j.actaastro.2012.11.002

Musk, E., 2017 Making life multiplanetary, 68th International Astronautical Congress. SpaceX, 28th September 2017.

NASA, 2017. *Space Debris and Human Spacecraft*. Available at: https://www.nasa.gov/mission_pages/station/news/orbital_debris.html (Accessed 1 October 2020)

NASA, 2021. *Frequently Asked Questions: Orbital debris*. Available at: https://www.nasa.gov/news/debris_faq.html (Accessed 19 February 2021)

NOAAA, 2021. *Space Weather Phenomena.* Available at: https://www.swpc.noaa.gov/phenomena (Accessed 19 February 2021)

Novák, A., 2010. *Sledovacie systémy v letectve*. 1. edition. Žilina: Žilinská univerzita. ISBN 978-80-554-0170-6.

[a]NSTS News reference manual, 1988. *Guidance, navigation and control.* Available at: https://science.ksc.nasa.gov/shuttle/technology/sts-newsref/sts-gnnc.html#sts-gnnc (Accessed 19 February 2021)

[b]NSTS News reference manual, 1988. *Orbital maneuvering system.* Available at: https://science.ksc.nasa.gov/shuttle/technology/sts-newsref/sts-oms.html (Accessed 19 February 2021)

Peterson, G., Sorge, M., Ailor, W., 2018. *Space traffic management in the age of new space*. Available at: https://aerospace.org/sites/default/files/2018-05/SpaceTrafficMgmt_0.pdf (Accessed 28 September 2020).

REACTION ENGINES, 2019. *Reaction Engines test programme fully validates precooler at hypersonic heat conditions*. Available at: https://www.reactionengines.co.uk/news/news/reaction-engines-test-programme-fully-validates-precooler-hypersonic-heat-conditions (Accessed 7 October 2020).

Santoro, T. et al., 2020. Spaceport and Ground segment assessment for enabling operations of suborbital transportation systems in the Italian territory. Acta Astronautica 152. 396-407. https://doi.org/10.1016/j.actaastro.2018.08.014

Sgobba, T., ALLAHDADI, F.A. 2013. Chapter 8 – Orbital Operations Safety. Safety Design for Space Operations. 411-602. https://doi.org/10.1016/B978-0-08-096921-3.00008-8

Sheetz, M., 2020. *There's big demand among the high net worth for Virgin Galactic spaceflights, Cowen survey shows*. Available at: https://www.cnbc.com/2020/08/31/virgin-galactic-cowen-survey-of-high-net-worth-individuals-for-spaceflight.html (Accessed 2 October 2020).

Spaceport America, 2020. *Launching your vehicle*. Available at: https://www.spaceportamerica.com/business/launch/ (Accessed 5 October 2020).

Škultéty, F., Čerňan, J., Rostáš, J., 2019. Proposal of the technical solution for location of BRS system, AEROjournal 13, Issue 1. 8-11. https://doi.org/10.26552/aer.J.2019.1

Treaty on Principles Governing the Activities of States in the Exploration and Use of Outer Space, including the Moon and Other Celestial Bodies (Outer Space Treaty), 19 December 1966, resolution 2222 (XVIII), (entered into force 10 October 1967).

Tullmann, R. et al., 2017. *On the Implementation of a European Space Traffic Management System*. Available at: https://www.dlr.de/gfr/Portaldata/59/Resources/intern/galileo/air_meets_space_solutions/STM_tuellmann_etal_2017_1_WhitePaper.pdf (Accessed 28 September 2020).

Yi-Wei Chang, E., 2020. From aviation tourism to suborbital space tourism: A study on passenger screening and business opportunities. Acta Astronautica 177. 410-420. https://doi.org/10.1016/j.actaastro.2020.07.020

Zahari, A.R., Romli, F.I., 2019. Analysis of suborbital flight operation using PESTLE. Journal of Atmospheric and Solar-Terrestrial Physics. 192, 104901. https://doi.org/10.1016/j.jastp.2018.08.006

https://doi.org/10.26552/aer.C.2020.2.5

NEW REGULATIONS FOR UAS FLIGHTS

INFORMATIVE ARTICLE

Branislav Kandera
Air Transport Department
University of Žilina
Univerzitná 8215/1
010 26, Žilina
branislav.kandera@ fpedas.uniza.sk

Filip Škultéty
Air Transport Department
University of Žilina
Univerzitná 8215/1
010 26, Žilina
filip.skultety@fpedas.uniza.sk

Benedikt Badánik
Air Transport Department
University of Žilina
Univerzitná 8215/1
010 26, Žilina
benedikt.badanik@ fpedas.uniza.sk

Abstract

The paper deals with the legislation in the field of unmanned aircraft systems (UAS) in the Slovak Republic. The main goal of the paper is to analyse the current legislative framework, which sets the basic rules and restrictions. The article's contribution is a description of the latest Implementing Regulation (EU) 2019/947. The solution to the issue consists of an analysis of the requirements for changes in current legislation based on people's experience from practice. The reason for the changes is to facilitate flying with UAS for all user groups, provided that safety is maintained, and risks are minimised. These new regulations are causing the most significant changes, especially for organisations that will perform aerial work with the UAS in the Specific category. These organisations need to transform their operations manuals and extend the aerial work system with a risk analysis.

Keywords

UAS, legislation, EASA, Slovak Republic, operation, implementing regulation

1. Introduction

The new European legislation has brought significant changes to UAS air traffic. On the one hand, it simplifies the possible commercial operation of "hobby pilots". On the other hand, it requires a marked change in previously approved aviation organisations' procedures through the UAS.

This article provides an overview of the new European legislation that is coming into force across the EU Member States. The first part is devoted to Decision No. 2/2019 issued by the Transport Authority of the Slovak Republic. It describes the common rules of category A3 and category B. It is followed by an explanation of the latest EC implementing regulations. These Regulations are described in terms of novelty.

1.1. Literature review

Following documents, Decision No 2/2019; Commission Implementing Regulation (EU) 2019/947) and Commission Implementing Regulation (EU) 2019/945) are an essential part of the studied material. In addition, the following articles were studied, which dealt with UAS concerning their various uses within the applicable regulations.

UAS regulations review by Pecho et al. was done during scrutiny of technology in the process of UAV missions. Ažaltovič et al. (2020) calculated the ground casualty risk during aerial work of Unmanned Aerial Vehicles in the urban areas. Regulations for UAS operations were considered in the flight inspection scope with unmanned aircraft (Novák et al., 2020). Unmanned Aircraft Vehicle Flight Precision was measured by Sedláčková, A.N. et al. (2020).

2. Decision No 2/2019

The Transport Authority, as a state administration body competent pursuant to § 7 par. 2 of Act No 143/1998 on Civil Aviation (Aviation Act) and on Amendments to Certain Acts, as amended later regulations, in conjunction with Art. 1 par. 4 of Commission Implementing Regulation (EU) No Regulation (EU) No 923/2012 of 26 September 2012 laying down common rules of the air and operating provisions for air traffic services and procedures and amending Implementing Regulation (EU) No 216/2008 1035/2011 and Regulation (EC) No 1265/2007, (EC) No 1794/2006, (EC) No 730/2006, (EC) No 1033/2006 and (EU) No 255/2010, as amended, taking into account Annex IX of Regulation (EU) 2018/1139 of the European Parliament and of the Council from 4 July 2018 on common rules in the field of civil aviation, establishing a European Union Aviation Safety Agency and amending Regulation (EC) No 2111/2005, (EC) No 1008/2008, (EU) No 996/2010, (EU) No 376/2014 and Directives 2014/30/EU and 2014/53/EU of the European Parliament and of the Council and repealing Regulations (EC) No 552/2004 and (ES) No 216/2008 and Council Regulation (EC) No 3922/912 and respecting other special regulations, determines in agreement with the Ministry of Defence of the Slovak Republic the conditions of the flight of unmanned aircraft in the airspace of the Slovak Republic.

For the purposes of this Decision, the following definitions shall apply:

(a) autonomous aircraft means an unmanned aircraft equipped with an independent control system that does not allow human intervention in the aircraft's control during flight.

(b) remotely piloted aircraft (unmanned pilot-operated aircraft) from a control station not located onboard the aircraft.

(c) model aircraft means an aircraft model according to a special regulation with or without an engine, which is not equipped with a device enabling automatic flight to a designated place, is controlled by a pilot at a distance throughout the flight by a control station and with which the pilot maintains direct visual contact.

Unmanned aircraft system (UAS) flight means any unmanned aerial vehicle operation from start-up, take-off to landing. Automatic flight means a method of conducting a flight by an unmanned aircraft, during which the unmanned aircraft independently performs predetermined turns or flight tasks, the remote pilot being able to intervene in the control of the unmanned aircraft at any time.

2.1. UAS categories

- Class C0 UAS, a remotely piloted aircraft or an aircraft model with a maximum take-off mass not exceeding 250 g,
- Class C1 UAS, a remotely piloted aircraft or an aircraft model with a maximum take-off mass, which is greater than 250 g and does not exceed 900 g,
- Class C2 UAS, a remotely piloted aircraft or an aircraft model with a maximum take-off mass, which is greater than 900 g and does not exceed 4 kg,
- Class C3 UAS a remotely piloted aircraft with a maximum take-off mass, which is greater than 4 kg and does not exceed 25 kg and has a typical size of less than 3 m,
- Class C4 UAS, an aircraft model with a maximum take-off mass, which is greater than 4 kg and does not exceed 25 kg,

2.2. General conditions for UAS flight

ACCORDING TO A SPECIAL REGULATION, an UAS flight may be performed if the basic requirements comply with the following rules.

A pilot must not fly an UAS if he/she is under the influence of a psychoactive substance. Flight by an UAS may be performed in uncontrolled airspace of class G at a maximum height of 120 m (400 ft) above the highest obstacle within a radius of 30 m (0.016 NM) from UAS; this does not apply in the case of a flight within an Aerodrome Traffic Zone (ATZ) in coordination with the aerodrome's operator. An UAS must not be equipped with a pulsating or rocket engine; this does not apply if the rocket engine is used for take-off. The flight by an UAS shall be performed so that the safety of other aircraft, persons and property on the ground is not endangered and that the protection of the environment against noise and emissions from pollutants is ensured. The prohibition of endangering other aircraft does not apply to each other between remotely piloted aircraft models subject to the participating UAS pilots' prior agreement and adopting appropriate safety measures. The UAS pilot must observe the surroundings, obstacles, and air traffic and avoid them. If an emergency occurs during a flight, the UAS pilot must immediately safely terminate the flight. An UAS may not be used to perform commercial air transport. An unmanned aircraft shall not be used to spray chemicals or for dropping objects; this does not apply in the case of aerial work, which may be performed only based on a permit from the Transport Authority issued in accordance with a special regulation.

An UAS pilot is obliged to thoroughly acquaint himself/herself with actual conditions in accordance with:

(a) the meteorological situation at the place of flight,

(b) use of airspace at the time and place of the flight,

(c) the operating conditions of the UAS,

(d) the manufacturer's instructions for the safe operation of the UAS,

(e) the UAS airworthiness and performance limitations,

(f) the flight procedures and emergency procedures specified by the manufacturer.

It is prohibited to operate an UAS at night unless otherwise provided. A flight may not be conducted within specified horizontal boundaries, and vertical boundaries of restricted airspace activated restricted airspace, temporarily segregated airspace, and temporarily reserved airspace. Unmanned Aerial Vehicles Classes C0 to C4 and UAS with a maximum take-off mass 25 kg or more shall be equipped with a back-up radio communication and control system which, in the event of loss of signal or failure, shall make a safe forced landing or shut down the engine and set rudders to a predefined position.

2.3. Operation subcategory A3

UAS 'open' operations category is divided into three subcategories A1, A2 and A3, based on operational limitations, requirements for the remote pilot and technical requirements for UAS. For the purposes of this study, the A3 category is analysed. The UAS flight may be conducted:

(a) at a minimum distance of 50 m (0.027 NM) from third persons in such a way, they are not endangered by the operation (considering the propulsion and performance of the UAV).

(b) in meteorological conditions for flight in visibility, unless otherwise specified,

(c) maintaining direct visual contact with the UAS,

(d) at a horizontal distance not more than 1 000 m (0.54 NM) from the pilot at a distance,

(e) in an aerodrome control zone (CTR) without coordination with the appropriate air traffic control unit at a minimum distance 5.6 km (3 NM) from the aerodrome reference point (ARP) and up to a height not more than 30 m above ground level (AGL),

(f) in such a way that densely populated areas of cities, municipalities, zones or urban concentrations, gatherings of people in the open air, buildings, airport protection zones, protection zones of

aeronautical ground facilities or protected areas are not flown,

(g) provided that the pilot with an UAS (with a maximum take-off mass 20 kg or more) has insurance for the damage caused by the operation to third parties.

2.4. Operation category B

An UAS flight under the conditions of operation category B may be performed in accordance with the general flight conditions referred in 2.2. and:

(a) with the approval of the Transport Authority and the conditions specified for the operation of the UAS, unless otherwise provided at night; if the drone is equipped with adequate lighting; in controlled airspace, if the drone flight is coordinated with the air traffic control unit; at a distance less than 50 m from third persons; and fly UAS with a maximum take-off mass of more than 25 kg.

(b) provided that the operator of the UAS concludes and fulfils a contract of liability insurance for the damage caused by the UAS operation; keep a logbook or a document replacing it; holds a license to fly an unmanned aerial vehicle and a certificate of UAS registration.

(c) apply for flight permission 30 days before the estimated date of the flight. Attached to the application is also a risk analysis, prepared according to the procedure published on the Transport Authority website, which contains particular requirements (Transport authority, 2019).

3. Regulation (EU) 2019/947

Commission Implementing Regulation (EU) 2019/947 of 24 May 2019 on the rules and procedures for the operation of unmanned aircraft is a new regulation which Slovak Republic adopted from 1 January 2021 having regard to Regulation (EU) 2018/1139 of the European Parliament and of the Council of 4 July 2018 on common rules in the field of civil aviation and establishing a European Union Aviation Safety Agency, and amending Regulations (EC) No 2111/2005, (EC) No 1008/2008, (EU) No 996/2010, (EU) No 376/2014 and Directives 2014/30/EU and 2014/53/EU of the European Parliament and the Council, and repealing Regulations (EC) No 216/2008 and (EC) No 552/2004 of the European Parliament.

3.1. Categories of UAS operations

UAS operations shall be performed in the 'open', 'specific' or 'certified' category defined as follows:

(a) UAS operations in the 'open' category shall not be subject to any prior operational authorisation, nor to an operational declaration by the UAS operator before the operation takes place;

(b) UAS operations in the 'specific' category shall require an operational authorisation issued by the competent authority or an authorisation received in accordance with conditions to be made by a UAS pilot;

(c) UAS operations in the 'certified' category shall require the certification of the UAS according to Delegated Regulation (EU) 2019/945 and the certification of the operator and, where applicable, the licensing of the remote pilot.

3.1.1. 'Open' category of UAS operations

Operations shall be classified as UAS operations in the 'open' category only where the following requirements are met:

(a) the UAS belongs to one of the classes set out in Delegated Regulation (EU) 2019/945 or is privately built or meets the conditions defined in Article 20;

(b) the unmanned aircraft has a maximum take-off mass of less than 25 kg;

(c) the remote pilot ensures that the unmanned aircraft are kept at a safe distance from people and that it is not flown over assemblies of people;

(d) the remote pilot keeps the unmanned aircraft in VLOS at all times except when flying in follow-me mode or when using an unmanned aircraft observer as specified;

(e) during flight, the unmanned aircraft is maintained within 120 metres from the closest point of the surface of the earth, except when overflying an obstacle, as specified;

(f) during flight, the unmanned aircraft does not carry dangerous goods and does not drop any material.

3.1.2. 'Specific' category of UAS operations

The competent authority shall specify whether the operational authorisation concerns:

(a) the approval of a single operation or more operations specified in time or location(s) or both. The operational authorisation shall include the precise associated list of mitigating measures;

(b) the approval of a 'light UAS operator certificate' (LUC), in accordance with part C of the Annex.

The UAS operator submits a declaration to the competent authority of the Member State of registration according to point UAS.SPEC.020 laid down in Part B of the Annex for an operation complying with a standard scenario as defined. The UAS operator shall not be required to obtain an operational authorisation in accordance with regulation.

An operational authorisation or a declaration shall not be required for:

(a) UAS operators are holding a LUC with appropriate privileges in accordance with point UAS.LUC.060 of the Annex;

(b) operations conducted in the framework of model aircraft clubs and associations that have received authorisation.

3.1.3. 'Certified' category of UAS operations

Operations shall be classified as UAS operations in the 'certified' category only where the following requirements are met the UAS is certified according to points (a), (b) and (c) of paragraph 1 of Article 40 of Delegated Regulation (EU) 2019/945; and the operation is conducted in any of the following conditions:

(a) over assemblies of people;

(b) involves the transport of people;

(c) involves the carriage of dangerous goods that may result in high risk for third parties in case of an accident.

Besides, UAS operations shall be classified as UAS operations in the 'certified' category where the competent authority, based on the risk assessment, considers that the risk of the operation cannot be adequately mitigated without the certification of the UAS and of the UAS operator and, where applicable, without the licensing of the remote pilot (Commission Implementing Regulation (EU) 2019/947).

3.2. Operation open subcategory A3

UAS operations in subcategory A3 shall comply with all of the following conditions:

(a) be conducted in an area where the remote pilot reasonably expects that no uninvolved person will be endangered within the range where the unmanned aircraft is flown during the entire time of the UAS operation;

(b) be conducted at a safe horizontal distance of at least 150 metres from residential, commercial, industrial or recreational areas;

(c) be performed by a remote pilot who has completed an online training course and passed an online theoretical knowledge examination as defined;

(d) be performed with an unmanned aircraft that has an MTOM, including payload, of less than 25 kg, in the case of a privately built UAS, or is marked as class C2 and is operated with active and updated direct remote identification and geo-awareness systems or; is marked as class C3 and is operated with active and updated direct remote identification and geo-awareness systems; or is marked as class C4.

3.3. Operation specific category

The UAS operator shall provide the competent authority with an operational risk assessment for the intended operation in accordance with general rules or submit a declaration when pointing UAS.SPEC.020 is applicable unless the operator holds a LUC with the appropriate privileges. The UAS operator shall regularly evaluate the adequacy of the mitigation measures taken and update them where necessary.

he UAS operator may submit an operational declaration of compliance with a standard scenario concerning operations of unmanned aircraft with:

(a) maximum characteristic dimension up to 3 metres in VLOS over;

(b) maximum characteristic dimension up to 1 metre in VLOS except over assemblies of people;

(c) maximum characteristic dimension up to 1 metre in BVLOS over sparsely populated areas;

(d) maximum characteristic dimension up to 3 metres in BVLOS

(e) performed below 120 metres from the earth's surface and in uncontrolled airspace (class F or G), or controlled airspace after coordination and individual flight authorisation in accordance with published procedures for the area of operation.

A declaration of UAS operators shall contain administrative information about the UAS operator, stating that the operation satisfies the operational requirement. The UAS operator's commitment to comply with the relevant mitigation measures required for the operation's safety, including the associated instructions for the operation, for the design of the unmanned aircraft and the competency of involved personnel.

Confirmation by the UAS operator that an appropriate insurance cover will be in place for every flight made under the declaration if required by Union or national law. Upon receipt of the declaration, the competent authority shall verify that the declaration contains all the elements and shall provide the UAS operator with a confirmation of receipt and completeness without undue delay. After receiving the confirmation of receipt and completeness, the UAS operator is entitled to start the operation.

UAS operators shall notify, without any delay, the competent authority of any change to the information contained in the operational declaration that they submitted. UAS operators holding a LUC with appropriate privileges are not required to submit the declaration (Commission Implementing Regulation (EU) 2019/945).

4. Conclusions

These new regulations are causing the most significant changes, especially for organisations that will perform aerial work with the UAS in the Specific category. These organisations need to transform their operations manuals and extend the aerial work system with a risk analysis. The situation is more straightforward when operating in the 'open ' category.

From 31 December 2020 to 1 January 2023, it is possible to fly UAS without a class Identification label in the 'open' category under the following conditions:

- UAS with less than 500 g MTOM cannot fly over people, and National Aviation Authority determines pilot competency;

- drones with less than 2 kg MTOM can fly 50 metres or more (horizontally) from people, and the pilot must undergo training equivalent to subcategory A2 (see the FAQ section on training);
- drones with less than 25 kg MTOM can fly in areas free from people, 150 metres or more away from properties, and the pilot must undergo training equivalent to subcategory A3 (see the FAQ section on training).

After 1 January 2023, it is also possible to fly UAS without class identification labels, however, only under the following subcategories of operation, for which operator shall comply fully with:

- Subcategory A1 when the drone's maximum take-off weight (MTOM) is less than 250 g; or
- Subcategory A3 when the drone's maximum take-off weight is less than 25 kg.

On the other hand, the new regulation also makes it easier for ordinary pilots to create aerial photographs commercially using UAS in the open category.

Currently, in the Slovak Republic conditions, the biggest problem is the non-compliance of national legislation with the new European rules. The authority is currently working intensively on this harmonisation of regulations, and we can expect significant changes in national regulations in the near future.

Further research will focus on in-depth scrutiny of implementation regulations and analyse implementation options for different UAS operators.

Acknowledgement

This publication was supported by the operational orogram Integrated infrastructure within the project: ***Inteligentné operačné a spracovateľské systémy pre UAV, kód ITMS2014+: 313011V422*** and co-financed by the European Regional Development Fund.

References

Ažaltovič, V., Škvareková, I., Pecho, P., Kandera, B., 2020. Calculation of the Ground Casualty Risk during Aerial Work of Unmanned Aerial Vehicles in the Urban Environment. In: Transportation Research Procedia, 2020, 44, pp. 271–275

Bugaj, M., Novak, A., Stelmach, A., Lusiak, T., 2020. Unmanned Aerial Vehicles and Their Use for Aircraft Inspection. In: Proceedings of the 22nd International Conference on New Trends in Civil Aviation 2020, NTCA 2020, 2020, pp. 45–50

European Commission, 2019. Implementing Regulation (EU) No 2019/947

European Commission, 2019. Implementing Regulation (EU) No 2019/945

Novák, A., Novák Sedlacková, A., Kandera, B., Lusiak, T., 2020. Flight inspection with unmanned aircraft. In: Transport Means - Proceedings of the International Conference, 2020, 2020-September, pp. 589

Pecho, P., Magdolenová, P., Bugaj, M., 2019. Unmanned aerial vehicle technology in the process of early fire localisation of buildings. In: Transportation Research Procedia, 2019, 40, pp. 461–468

Sedláčková, A.N., Kurdel, P., Labun, J., 2020. Simulation of Unmanned Aircraft Vehicle Flight Precision. In: Transportation Research Procedia, 2020, 44, pp. 313–320

Transport Authority, 2019. Regulation Decision No 2/2019

AERO*journal*

International Scientific Journal
Published by University of Žilina, Univerzitná 8215/1, 010 26 Žilina, The Slovak Republic
The Faculty of Operation and Economics of Transport and Communications
Air Transport Department

Head of the editorial board: **prof. Ing. Antonín Kazda, PhD.**
Editor in chief: **doc. Ing. Martin Bugaj, PhD.**
Technical editor: **Ing. Matúš Materna, PhD.**

Printed by: EDIS – Vydavateľstvo Žilinskej univerzity v Žiline, Univerzitná 8215/1, Žilina
Circulation: 100 prints

https://doi.org/10.26552/aer.J.2020.2
ISSN: 1338-8215